

CONSTANT MEAN CURVATURE SURFACES FROM RING PATTERNS: GEOMETRY FROM COMBINATORICS

ALEXANDER I. BOBENKO, TIM HOFFMANN AND NINA SMEENK

ABSTRACT. We define discrete constant mean curvature (cmc) surfaces in the three-dimensional Euclidean and Lorentz spaces in terms of sphere packings with orthogonally intersecting circles. These discrete cmc surfaces can be constructed from orthogonal ring patterns in the two-sphere and the hyperbolic plane. We present a variational principle that allows us to solve boundary value problems and to construct discrete analogues of some classical cmc surfaces. The data used for the construction is purely combinatorial - the combinatorics of the curvature line pattern. In the limit of orthogonal circle patterns we recover the theory of discrete minimal surfaces associated to Koebe polyhedra all edges of which touch a sphere. These are generalized to two-sphere Koebe nets, i.e., nets with planar quadrilateral faces and edges that alternately touch two concentric spheres.

1. INTRODUCTION

In the last two decades, the field of discrete differential geometry emerged on the border of differential and discrete geometry, see the books [20, 19, 10, 23, 27]. Whereas classical differential geometry investigates smooth geometric shapes (such as surfaces), and discrete geometry studies geometric shapes with a finite number of elements (polyhedra), discrete differential geometry aims at a development of discrete equivalents of the geometric notions and methods of surface theory. The latter appears then as a limit of the refinement of the discretization. Current progress in this field is to a large extent stimulated by its relevance for computer graphics and visualization.

One of the central problems of discrete differential geometry is to find proper discrete analogues of special classes of surfaces, such as minimal, constant mean curvature, isothermic, etc. Usually, one can suggest various discretizations with the same continuous limit which have quite different geometric properties. The goal of discrete differential geometry is to find a discretization which inherits as many essential properties of the smooth geometry as possible.

Our discretizations are based on quadrilateral meshes, i.e., we discretize parametrized surfaces. For the discretization of a special class of surfaces, it is natural to choose an adapted parametrization. In this paper, we consider discretizations in terms of circles and spheres, which are treated as conformal curvature line discretizations of surfaces, and develop a method to investigate a discrete model for constant mean curvature (cmc) surfaces.

Date: October 14, 2024.

Key words and phrases. discrete differential geometry, constant mean curvature, minimal surfaces, circle patterns, ring patterns, variational principles.

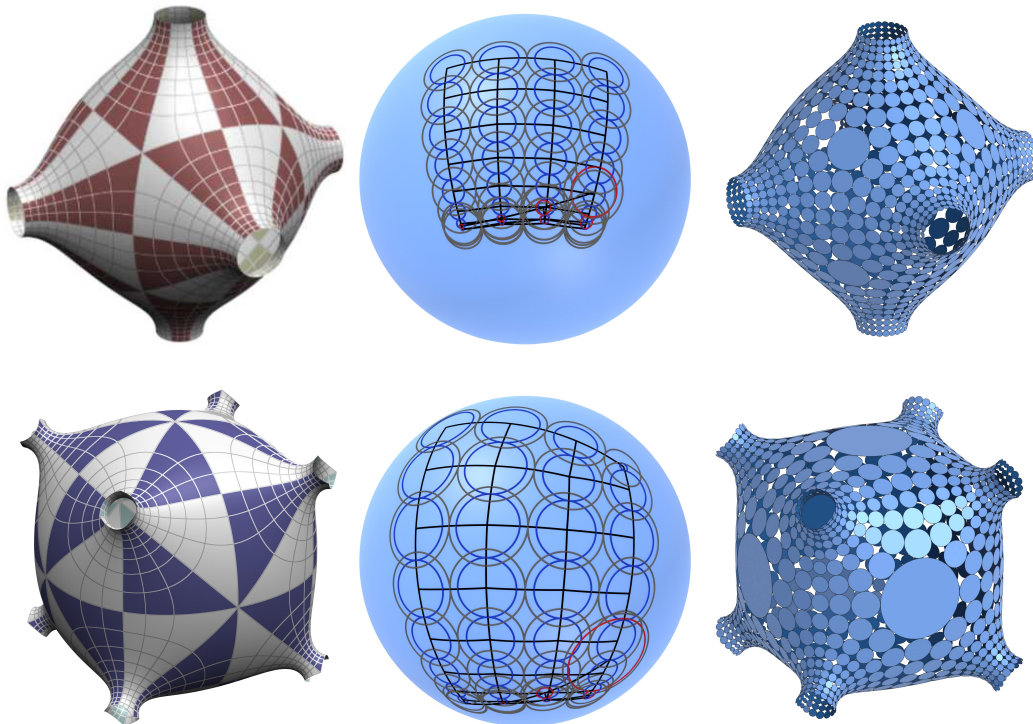


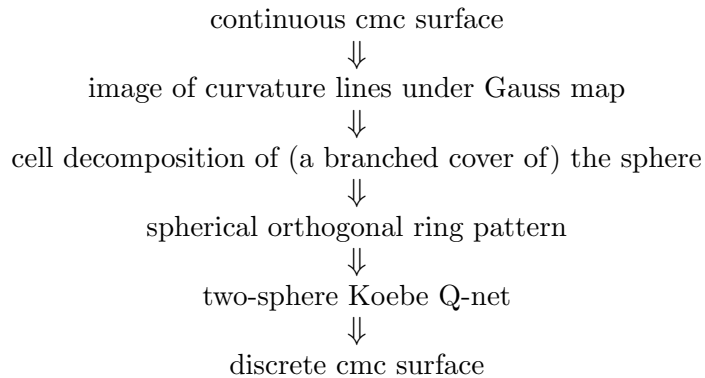
Figure 1. Triply periodic cmc surfaces in \mathbb{R}^3 : Schwarz's P surface (first line) and Schoen's I-WP surface (second line). The left column presents the smooth cmc surfaces from [13] obtained by the loop group method from the theory of integrable systems. The right column are the corresponding discrete cmc surfaces built by touching disks. Their spherical orthogonal ring patterns are shown in the middle.

We consider cmc surfaces as a subclass of isothermic surfaces. The analogous discrete surfaces, *discrete S -isothermic surfaces* [17, 20] consist of touching spheres, and of circles which intersect the spheres orthogonally in their points of contact, see Section 2 and Fig. 4. Isothermic surfaces are described by integrable equations, and thus belong to integrable differential geometry [22, 7]. They allow Darboux transformations and a duality transformation, called the Christoffel transformation. Smooth cmc surfaces s are characterized among isothermic surfaces by the property that their Christoffel dual s^* is simultaneously a Darboux transform [32]. In this case these surfaces are parallel, and define a common Gauss map $n = s^* - s$. The transformations and the characterization of cmc surfaces carry over to the discrete domain. Thus, one arrives at the notion of *discrete S -isothermic cmc surfaces* [35, 14], or *discrete cmc surfaces* for short. This definition is in complete agreement with the notion of discrete curvatures, see [18], defined for polyhedral surfaces using a discrete version of the classical Steiner formula. Indeed, Theorem 3.9 claims that the discrete mean curvature of the pair (s, n) is constant.

As we show in Section 3, the role of the Gauss maps n is played by a so called two-sphere Koebe net, a polyhedral surface with planar quadrilateral faces, all edges of which alternatively touch two concentric spheres S_{\pm}^2 . This is a generalization of a classical Koebe polyhedron, all edges of which touch a common sphere S^2 . Koebe polyhedra are in one to

one correspondence with orthogonal circle patterns on S^2 . Using this identification, Koebe [38] has shown that any 3-dimensional combinatorial convex polytope can be (essentially uniquely) realized as a Koebe polyhedron. For generalizations and proofs of this theorem see [21, 48, 46, 8], the latter also for a variational proof. In Section 4 we show that two-sphere Koebe nets are in one to one correspondence to orthogonal ring patterns on a sphere. The latter were described analytically in [11], including a variational description generalizing the description of orthogonal circle patterns. We present it in Section 5. The variational principle allows us to construct particular orthogonal ring patterns determined by their combinatorics and also by some geometric boundary conditions.

This leads to a construction method for discrete S-isothermic cmc surfaces from orthogonal ring patterns. Our general method to construct discrete cmc surfaces is schematically shown in the following diagram, see also Section 6:



As usual in the theory of minimal and cmc surfaces [34], one starts constructing such a surface with a rough idea of how it should look. To use our method, one should understand the symmetries of its Gauss map and the *combinatorics* of the curvature line pattern. The image of the curvature line pattern under the Gauss map provides us with a cell decomposition of (a part of) S^2 or a covering. From these data we obtain a spherical orthogonal ring pattern with the prescribed combinatorics. Finally, a direct construction, see Theorem 6.1, recovers the pair s, s^* of Christoffel dual cmc surfaces from their common Gauss map $n = s^* - s$.

Let us emphasize that our data, besides possibly boundary conditions, are purely combinatorial – the combinatorics of the curvature line pattern. All faces are quadrilaterals and typical vertices have four edges. There may exist distinguished vertices (corresponding to the ends or umbilic points of a cmc surface) with a different number of edges.

The most nontrivial step in the above construction is the third one listed in the diagram. It is based on the variational description of ring patterns. Under some constraints (see Sections 6 and 7) it implies the existence and uniqueness for the discrete cmc S-isothermic surface under consideration, but not only this. This principle provides us with a variational description of discrete cmc S-isothermic surfaces and makes possible a solution of some Plateau problems as well. It is also an effective tool for numerically constructing these surfaces.

In the limit of the zero mean curvature $H = 0$, the two spheres coincide $S^2_{\pm} = S^2$, the ring patterns become circle patterns, and we recover the theory of discrete minimal surfaces developed in [15]. We describe this limit in Section 7 and show that a generic discrete

minimal surface possesses a one parameter deformation family of discrete cmc surfaces, parametrized by (small) H . This corresponds to a deformation of a circle pattern to ring patterns with the same combinatorial and boundary data and varying “thickness” parameter.

In Section 8 we apply our method to construct some examples of periodic, reflectionally symmetric discrete cmc surfaces. In particular, we construct discrete cmc analogues of minimal surfaces of Schwarz and Schoen, shown in Fig. 1. The surfaces are composed of touching disks. The touching coins lemma (see [15]) ensures the existence of orthogonal spheres passing through their touching points. Without changes our method can be applied to construct cmc analogs of numerous discrete minimal surfaces found in [12]. For constructing one should simply replace the variational functional for circle patterns by the corresponding functional for ring patterns (see Section 5 and [8]), with the same convexity properties. Note that rotationally symmetric discrete cmc surfaces (discrete Delaunay surfaces) were previously constructed in [14] by unrolling the billiard in an ellipse. The isometric deformation of discrete cmc surfaces, known as the associated family, was geometrically described in [39]. In particular the associated family of discrete Delaunay surfaces was constructed. Discrete cmc surfaces have been applied in architectural geometry for construction of doubly-curved building envelopes [52].

The convergence of discrete minimal S-isothermic surfaces to smooth minimal surfaces was proven in [15], see also a visualization [16]. The proof is based on Schramm’s approximation result for circle patterns with the combinatorics of the square grid [49]. Later it was shown in [40] that the convergence of minimal surfaces is in fact C^∞ , i.e., with all derivatives. Our numerical experiments with discrete cmc surfaces show an astonishingly good convergence, demonstrated in Fig. 1. It would be desirable to give a mathematical proof of this fact. The first step here is the approximation of (harmonic) Gauss maps by infinitesimal spherical orthogonal ring patterns shown in [11].

In Sections 9-13 we define and investigate spacelike discrete cmc surfaces in the Lorentz space $\mathbb{R}^{2,1}$. The considerations and results are quite similar to the Euclidean case. The main difference is that in this case the Gauss map n connecting s and s^* forms a spacelike two spheres Koebe net, which can be identified with an orthogonal ring pattern in the hyperbolic plane. Unlike the spherical case, the corresponding variational functional is convex, see Section 11 and [11]. This allows us to prove the existence and uniqueness of spacelike discrete cmc surfaces in $\mathbb{R}^{2,1}$ satisfying classical boundary conditions. Discrete maximal surfaces, which correspond to $H = 0$ and to hyperbolic orthogonal circle patterns, are considered in Section 13. Discrete spacelike maximal surfaces were recently linked to models in statistical mechanics [3, 4].

It was shown in [11] that spherical and hyperbolic orthogonal ring patterns are described by the integrable Q4-equation [2]. The latter is an equation with an elliptic spectral parameter, and is the master discrete integrable equation in the classification of [1]. This leads to an analytic description of discrete cmc surfaces in \mathbb{R}^3 and $\mathbb{R}^{2,1}$ in terms of loop groups. Known investigation methods of smooth cmc surfaces from an integrable point of view are mostly analytic. All integration methods, including the DPW factorization approach [24], algebro-geometric solutions [33, 9], are based on the loop group representations of the corresponding geometries. Although the DPW method was very productive in construction of new examples of cmc surfaces [28], precise mathematical proofs of their

existence turned out to be a difficult issue. Recent progress here was achieved for n-noids and surfaces of high genus [53, 29]. We do not explore the loop group description in the present paper and plan to address it in future publications. Here we expect a nice interplay of smooth and discrete theories enriching both.

Cmc-surfaces in \mathbb{R}^3 are isometric to minimal surfaces in S^3 . This fact, known as the Lawson correspondence [41], can be lifted to a relation for the frames of the corresponding surfaces [26]. The Lawson correspondence is a powerful method to investigate embedded cmc-surfaces, by constructing the corresponding minimal surfaces in S^3 , see for example [25]. Analogously, cmc-surfaces in $\mathbb{R}^{2,1}$ are isometric to minimal surfaces in three-dimensional anti-de Sitter space AdS_3 , which are popular models in the string theory. It is a natural important problem to find a discrete Lawson correspondence, which should be a geometric construction of discrete minimal surfaces in S^3 and AdS_3 consisting of touching disks, from orthogonal ring patterns in the sphere and the hyperbolic plane.

ACKNOWLEDGEMENTS

This research was supported by the DFG Collaborative Research Center TRR 109 “Discretization in Geometry and Dynamics”.

2. DISCRETE S-ISOTHERMIC SURFACES IN \mathbb{R}^3

Motivated by the combinatorics of the curvature lines on smooth surfaces we consider quad graphs with interior vertices of even valence, typically four. We denote these graphs by \mathcal{G} and their vertices, edges and faces by $V(\mathcal{G}), E(\mathcal{G})$ and $F(\mathcal{G})$ respectively. Recall that a quad graph is a quadrilateral cell decomposition of a surface, meaning all faces in $F(\mathcal{G})$ are quadrilaterals. A special case is a cell complex $\mathcal{G} \subset \mathbb{Z}^2$ defined by a subset of elementary squares of the \mathbb{Z}^2 lattice in \mathbb{R}^2 .

The edges of a graph \mathcal{G} can be combinatorially divided into ‘horizontal’ and ‘vertical’ edges, which we consistently label by i and j , see Figure 2. We denote the vertices of an elementary quadrilateral of \mathcal{G} by v, v_i, v_{ij} and v_j , where v is a vertex of \mathcal{G} , and v_i and v_j are its horizontal and vertical neighboring vertices, respectively. The vertex v_{ij} is the fourth vertex of the elementary quadrilateral.

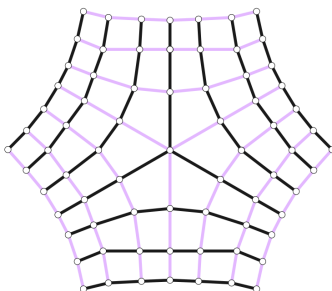


Figure 2. A quad graph \mathcal{G} with interior vertices of even valency. The edges are divided into ‘horizontal’ i -edges (black) and ‘vertical’ j -edges (pink), such that in each quadrilateral the edges alternately change color.

To proceed with the Möbius geometric characterization of S-isothermic nets, we recall some basic facts about Möbius geometry, see [30] and [20, Chapter 9].

Let $\mathbb{R}^{4,1}$ be the five-dimensional Lorentz-Minkowski space equipped with the non-degenerate bilinear form

$$(1) \quad \langle x, y \rangle_{4,1} = x_1y_1 + x_2y_2 + x_3y_3 + x_4y_4 - x_5y_5.$$

Let e_1, \dots, e_5 denote the standard basis of $\mathbb{R}^{4,1}$ and let $e_0 := \frac{1}{2}(e_5 - e_4)$ and $e_\infty := \frac{1}{2}(e_4 + e_5)$.

Points in $\mathbb{R}^3 \cup \{\infty\}$ can be identified with points in the *light cone*

$$\hat{\mathcal{S}}_0 := \{\hat{x} \in \mathbb{R}^{4,1} \mid \langle \hat{x}, \hat{x} \rangle_{4,1} = 0\}$$

via the identification

$$(2) \quad \mathbb{R}^3 \ni x \leftrightarrow \hat{x} = x + e_0 + \|x\|^2 e_\infty \in \hat{\mathcal{S}}_0.$$

In this context, x on the right hand side is understood as $x_1e_1 + x_2e_2 + x_3e_3 \in \mathbb{R}^{4,1}$, and points of the form $\hat{x} = x + e_0 + \|x\|^2 e_\infty \in \hat{\mathcal{S}}_0$ are normalized such that $\langle \hat{x}, e_\infty \rangle_{4,1} = -\frac{1}{2}$. The point $\infty \in \mathbb{R}^3 \cup \{\infty\}$ is identified with e_∞ .

If $\mathbb{R}^{4,1}$ is interpreted as the space of homogeneous coordinates of $\mathbb{R}P^4$, points in $\mathbb{R}^3 \cup \{\infty\}$ can be identified with the stereographic projection of points on

$$\mathcal{M} := \{[\hat{x}] \in \mathbb{R}P^4 \mid \langle \hat{x}, \hat{x} \rangle_{4,1} = 0\},$$

which is called the *Möbius quadric*. A point of the form (2) in $\hat{\mathcal{S}}_0$ represents a special choice of homogeneous coordinates for the corresponding projective point in \mathcal{M} . Similarly, points outside the Möbius quadric, i.e.,

$$[\hat{x}] \in \mathcal{M}_+ := \{[\hat{x}] \in \mathbb{R}P^4 \mid \langle \hat{x}, \hat{x} \rangle_{4,1} > 0\},$$

can be identified with non-oriented spheres in \mathbb{R}^3 . Hyperplanes are considered as spheres with infinite radius. A sphere with center c and radius d is represented by the projective point

$$[\hat{s}] = [c + e_0 + (\|c\|^2 - d^2)e_\infty] \in \mathcal{M}_+.$$

Its homogeneous coordinates can be normalized to

$$\hat{s} = \frac{1}{d} (c + e_0 + (\|c\|^2 - d^2)e_\infty)$$

on the Lorentz unit sphere

$$(3) \quad \hat{\mathcal{S}}_1 := \{\hat{x} \in \mathbb{R}^{4,1} \mid \langle \hat{x}, \hat{x} \rangle_{4,1} = 1\} \subset \mathbb{R}^{4,1}.$$

The sign of the radius d encodes the orientation of the sphere. Note that the spheres with different orientations $\pm d$ correspond to different points on $\hat{\mathcal{S}}_1$, but are represented by the same point in \mathcal{M}_+ .

General S-isothermic surfaces were introduced in [20] as two-dimensional T-nets in $\mathbb{R}^{4,1}$.

Definition 2.1. *A map*

$$s : V(\mathcal{G}) \rightarrow \{\text{oriented spheres in } \mathbb{R}^3\}$$

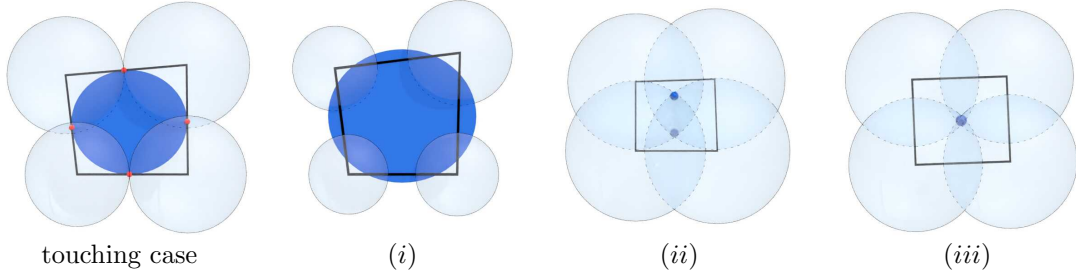


Figure 3. Three types of S-isothermic quadrilaterals with vertex spheres (i) possessing a common orthogonal circle, (ii) intersecting in two points, or (iii) intersecting in one point. The first image shows the special case of type (i) where vertex spheres touch.

is called a discrete S-isothermic surface if the corresponding map $\hat{s} : V(\mathcal{G}) \rightarrow \hat{\mathbb{S}}_1 \subset \mathbb{R}^{4,1}$, that maps oriented spheres to

$$\hat{s} = \frac{1}{d} (c + e_0 + (\|c\|^2 - d^2)e_\infty),$$

satisfies the discrete Moutard equation

$$\hat{s}_{v_{ij}} - \hat{s}_v = a_{ij}(\hat{s}_{v_j} - \hat{s}_{v_i}).$$

for some $a_{ij} : F(\mathcal{G}) \rightarrow \mathbb{R}$.

Remark. Instead of considering the Lorentz unit sphere (3) a sphere centered at the origin with an arbitrary radius

$$\hat{\mathbb{S}}_\kappa := \{\hat{x} \in \mathbb{R}^{4,1} \mid \langle \hat{x}, \hat{x} \rangle_{4,1} = \kappa\}$$

can be used to identify its points with oriented spheres in \mathbb{R}^3 . In this case the scaling factor of the homogeneous lift of a sphere \hat{s} is given by $\frac{\kappa}{r}$. In the limit $\kappa \rightarrow 0$ one obtains the original discrete isothermic surfaces introduced in [7]. Since we do not consider this convergence in the present paper we restrict ourselves to the fixed value $\kappa = 1$.

Note that \hat{s} is a *Q-net*, i.e., the vertices $\hat{s}_v, \hat{s}_{v_i}, \hat{s}_{v_{ij}}, \hat{s}_{v_j}$ are coplanar. The elementary quadrilaterals of S-isothermic surfaces are called *S-isothermic quadrilaterals*.

Corollary 2.2. *Let $s_v, s_{v_i}, s_{v_{ij}}$ and s_{v_j} be four the spheres of an S-isothermic quadrilateral. Then*

$$(4) \quad \begin{aligned} \langle \hat{s}_v, \hat{s}_{v_i} \rangle_{4,1} &= \langle \hat{s}_{v_j}, \hat{s}_{v_{ij}} \rangle_{4,1} =: \alpha_i \\ \langle \hat{s}_v, \hat{s}_{v_j} \rangle_{4,1} &= \langle \hat{s}_{v_i}, \hat{s}_{v_{ij}} \rangle_{4,1} =: \alpha_j. \end{aligned}$$

Further they satisfy one of the three conditions shown in Figure 3, namely

- (i) They have a common orthogonal circle;
- (ii) They intersect in exactly two points;
- (iii) They intersect in exactly one point.

Proof. As a Moutard net in the quadric \hat{S}_1 , the map \hat{s} admits the labeling property (4) [20]. The planarity of the faces of \hat{s} corresponds to the spheres around a face in \mathbb{R}^3 satisfying one of the conditions (i), (ii) or (iii). Let us consider the three-dimensional linear subspaces in $\mathbb{R}^{4,1}$ containing a face of \hat{s} . The induced metric on its orthogonal complements is either of signature (2, 0), (1, 1) or degenerate. These three cases correspond to the conditions (i), (ii) and (iii) respectively. For more details see [20]. \square

S-isothermic surfaces are discrete Koenigs nets and invariant under Möbius transformations. The edge labels α_i and α_j have the meaning of cosines of the intersection angles of the neighboring spheres, resp. of their so-called inversive distance, if they do not intersect.

If all quadrilaterals of an S-isothermic surface s are of the same type, s is said to be of type (i), (ii), or (iii). A special case of type (i), introduced in [17], are S-isothermic surfaces where neighboring vertex spheres touch, called S_1 -isothermic surfaces, see Figure 3 (left). In this case the orthogonal circles form inscribed circles of the quadrilaterals and neighboring circles touch in the same points as the spheres, see Figure 4. For the edge labels (4) of an S_1 -isothermic surface it is $\alpha_i, \alpha_j = \pm 1$. To ensure that $\alpha_i \neq \alpha_j$ for each quadrilateral, one chooses an orientation of spheres such that neighboring spheres are in non-oriented contact along horizontal edges and in oriented contact along vertical edges,

$$\begin{aligned}\alpha_i &= \langle \hat{s}_v, \hat{s}_{v_i} \rangle_{4,1} = \langle \hat{s}_{v_j}, \hat{s}_{v_{ij}} \rangle_{4,1} = -1 \\ \alpha_j &= \langle \hat{s}_v, \hat{s}_{v_j} \rangle_{4,1} = \langle \hat{s}_{v_i}, \hat{s}_{v_{ij}} \rangle_{4,1} = 1.\end{aligned}$$

Let

$$c : V(\mathcal{G}) \rightarrow \mathbb{R}^3, \quad v \mapsto c_v$$

denote the center net of the spheres of an S-isothermic net and let $d : V(\mathcal{G}) \rightarrow \mathbb{R}$ denote the corresponding signed radii. Any S-isothermic surface possesses a dual S-isothermic surface [20].

Lemma and Definition 2.3. *Let s be an S -isothermic surface. Then the \mathbb{R}^3 -valued discrete one-form ∂c^* defined by*

$$(5) \quad \partial_{(v,v')} c^* = \frac{\partial_{(v,v')} c}{d_v d_{v'}},$$

with $(v, v') \in E(\mathcal{G})$, is exact. Its integration defines (up to a translation) a function

$$c^* : V(\mathcal{G}) \rightarrow \mathbb{R}^3, \quad v \mapsto c_v^*.$$

Define also

$$d^* : V(\mathcal{G}) \rightarrow \mathbb{R}, \quad v \mapsto d_v^* = \frac{1}{d_v}.$$

Then the map

$$s^* : V(\mathcal{G}) \rightarrow \{\text{oriented spheres in } \mathbb{R}^3\}$$

with spheres with centers c^* and radii d^* is an S-isothermic surface, called Christoffel dual to s .

With the chosen orientation of spheres, the definition of the one-form (5) implies that horizontal edges maintain their orientation, while vertical edges reverse their orientation in the Christoffel dual.

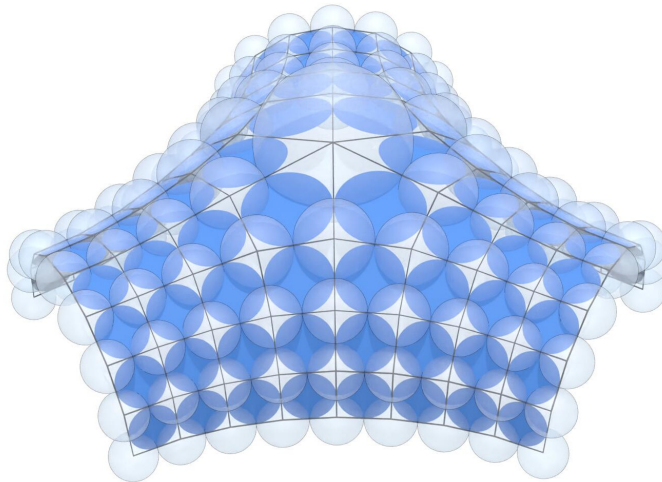


Figure 4. An S_1 -isothermic surface. Each quad possesses an incircle that intersects adjacent spheres orthogonally and passes through their touching points. The one large vertex sphere corresponds to an umbilic point, an inner vertex of \mathcal{G} with valency greater than four. The figure shows a piece of the doubly periodic S_1 -isothermic cmc surface $\psi(U_{2,2})$ presented in Section 8.

Corollary 2.4. *Christoffel duality preserves edge labels. In particular, it preserves the class of S_1 -isothermic surfaces.*

When extending the combinatorics of an S_1 -isothermic surface by introducing its face circle centers and its touching points as new vertices (referred to as the *central extension*), one obtains a related discrete isothermic surface [17]. In this extension, all faces of the isothermic surface form kites with one pair of opposite right angles. Dualizing the isothermic surface yields a dual isothermic surface that is itself the central extension of the Christoffel dual of the S_1 -isothermic surface. The following corollary is a direct consequence when considering the dual of the central extension.

Corollary 2.5. *The radii d_f and d_f^* of the orthogonal circles of an S_1 -isothermic surface and its Christoffel dual are related by*

$$d_f^* = \frac{1}{d_f}.$$

Sometimes it is more convenient to define the Christoffel up to scaling (and translation). In general, there exists an arbitrary global constant $\lambda \in \mathbb{R}$ such that

$$(6) \quad d_v d_v^* = d_f d_f^* = \lambda.$$

In Definition 2.3 we have fixed the scaling by choosing $\lambda = 1$.

3. DISCRETE CMC SURFACES IN \mathbb{R}^3

S-isothermic nets belong to integrable discrete differential geometry [20]. S-isothermic nets with underlying \mathbb{Z}^2 combinatorics can be extended consistently to the \mathbb{Z}^n lattice

so that all its two-dimensional coordinate subnets are S-isothermic. The generalization to the combinatorics of \mathcal{G} is straight forward. This property can be interpreted as a transformation of two-dimensional S-isothermic nets called *Darboux transform* [35, 20].

Definition 3.1. *Two S-isothermic surfaces s and s^+ are called a Darboux pair if the corresponding Moutard nets $\hat{s}, \hat{s}^+ : V(\mathcal{G}) \rightarrow \mathbb{R}^{4,1}$ are related by a Moutard transformation. In particular the transformation faces $(\hat{s}_v, \hat{s}_{v'}, \hat{s}_v^+, \hat{s}_{v'}^+)$ fulfill the Moutard equation*

$$\hat{s}_{v'}^+ - \hat{s}_v = a_+(\hat{s}_v^+ - \hat{s}_{v'})$$

with some $a_+ : E(\mathcal{G}) \rightarrow \mathbb{R}$. In this case, one surface is called a Darboux transform of the other.

A Darboux transform s^+ of an S-isothermic net s is uniquely determined by the choice of one of the spheres of s^+ . A Darboux transform has an associated constant parameter α , which arises from the edge labeling property of the Moutard equation:

$$(7) \quad -2\alpha := -2\langle \hat{s}_v, \hat{s}_v^+ \rangle_{4,1} = \|c_v - c_v^+\|^2 - (d_v^2 + d_v^{+2}).$$

Corollary 3.2. *Darboux transformations preserve edge labels. In particular, they preserve the class of S_1 -isothermic surfaces.*

Smooth cmc surfaces can be characterized through their Darboux and Christoffel transformations [32].

Theorem 3.3. *A smooth isothermic surface f is a surface of constant mean curvature $H \neq 0$ if and only if the (correctly scaled and positioned) Christoffel transform f^* is also a Darboux transform. In this case, f^* is the parallel surface at distance $\frac{1}{H}$.*

This characteristic property was used to define discrete isothermic surfaces of constant mean curvature [31] and S-isothermic cmc surfaces [35].

Definition 3.4. *An S-isothermic surface s is an S-isothermic surface of constant mean curvature, or S-cmc surface for short, if its Christoffel dual s^* is simultaneously a Darboux transform (after appropriate scaling and translation).*

The pair s, s^* of an S-cmc surface and its Christoffel dual is called an *S-cmc pair*.

3.1. The Gauss map of S_1 -cmc surfaces. We now restrict our considerations of S-cmc surfaces to the case of touching spheres, i.e., to S_1 -cmc surfaces.

The Gauss map of a smooth surface is a map to the unit sphere S^2 . Natural discretizations of Gauss maps are polyhedra with vertices on S^2 , faces tangent to S^2 , or edges tangent to S^2 . These discretizations lead to circular surfaces [18], conical surfaces [42, 45], and surfaces of Koebe type [15], respectively. Polyhedra with all edges touching S^2 are called *Koebe Polyhedra*, or *Koebe nets* when considering only local pieces. They are used to describe the Gauss map of S_1 -minimal surfaces [15]. A generalization of Koebe polyhedra to the case when all edges touch a general convex body was considered in [48].

For our purposes, we propose another generalization of Koebe nets by introducing two spheres concentric with the unit sphere and by considering nets that are alternately tangent to these two spheres, see Figure 5.

Definition 3.5. A Q -net $k : V(\mathcal{G}) \rightarrow \mathbb{R}^3$ is called a two-sphere Koebe net if its edges alternately touch two spheres S_+^2 and S_-^2 (concentric with the unit sphere S^2) whose radii satisfy the relation $r_+ r_- = 1$.

The latter condition ensures that the two spheres S_+^2 and S_-^2 and the discrete net k remain close to the unit sphere. Indeed, S_-^2 can be obtained by a sphere inversion of S_+^2 in S^2 , and vice versa.

Theorem 3.6. Let s and s^* be a (suitably scaled) S_1 -cmc pair. The Gauss map

$$(8) \quad n : V(\mathcal{G}) \rightarrow \mathbb{R}^3, \quad v \mapsto n_v := c_v^* - c_v,$$

between the sphere centers of s and s^* , forms a two-sphere Koebe net.

Before proving this theorem, we will investigate the properties of edge and face normals of an S_1 -cmc pair. To that end, let $t, t^* : E(\mathcal{G}) \rightarrow \mathbb{R}^3$ denote the points of contact between neighboring spheres on primal and dual edges, as illustrated in the Figures 6 and 7.

Proposition 3.7. The edge normals

$$(9) \quad l : E(\mathcal{G}) \rightarrow \mathbb{R}^3, \quad (v, v') \mapsto l_{(v,v')} := t_{(v,v')}^* - t_{(v,v')},$$

which connect the points of contact on primal and corresponding Christoffel dual edges, are orthogonal to both primal and dual edges,

$$(10) \quad l_{(v,v')} \perp c_{v'} - c_v \quad \text{and} \quad l_{(v,v')} \perp c_{v'}^* - c_v^*.$$

Additionally, the edge normals have constant length:

$$(11) \quad \|l_{(v,v')}\|^2 = \begin{cases} -2\alpha + 2\lambda & \text{for embedded faces} \\ -2\alpha - 2\lambda & \text{for non-embedded faces.} \end{cases}$$

Here α denotes the parameter of the Darboux transform (7) and λ represents the global constant (6).

Proof. The transformation faces of an S_1 -cmc pair form S-isothermic trapezoids: S-isothermic quadrilaterals with an orthogonal circle and one pair of parallel edges, see Figure 6. The

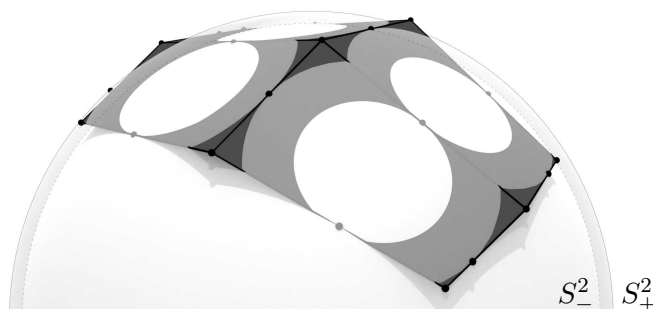


Figure 5. A two-sphere Koebe net. Its edges alternately touch the larger, transparent gray sphere S_+^2 and the smaller, white sphere S_-^2 .

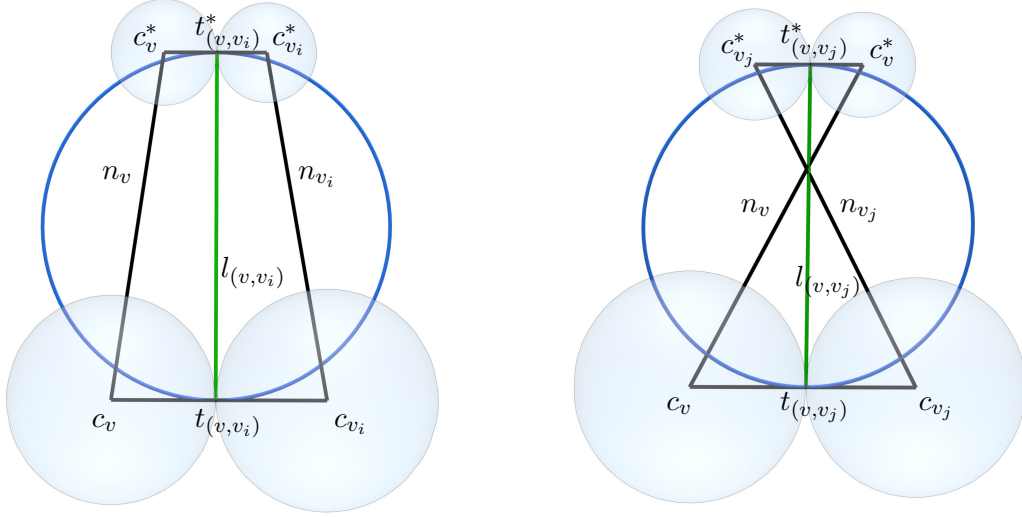


Figure 6. The two types of transformation faces of an S_1 -cmc pair together with vertex normals (black), edge normals (green) and the circle orthogonal to the four adjacent vertex spheres (blue). Embedded faces correspond to horizontal edges, non-embedded faces correspond to vertical edges.

parallel edges, $c_{v'} - c_v$ and $c_{v'}^* - c_v^*$, are tangent to the orthogonal circle, with the points of tangency at $t_{(v,v')}$ and $t_{(v,v')}^*$. This implies (10).

To prove the second part of the proposition, we observe that the edge normals are also tangent to both the primal and dual spheres at the points $t_{(v,v')}$ and $t_{(v,v')}^*$. Using the orthogonality (10), we can compute the squared length of the edge normals as follows:

$$\begin{aligned} \|c_{v_i} - c_{v_i}^*\|^2 - (d_{v_i} - d_{v_i}^*)^2 &= \|c_{v_i} - c_{v_i}^*\|^2 - (d_{v_i}^2 + d_{v_i}^{*2}) + 2\lambda, \\ \|c_{v_j} - c_{v_j}^*\|^2 - (d_{v_j} + d_{v_j}^*)^2 &= \|c_{v_j} - c_{v_j}^*\|^2 - (d_{v_j}^2 + d_{v_j}^{*2}) - 2\lambda, \end{aligned}$$

for embedded and non-embedded transformation faces, respectively. A comparison with (7) leads to (11). \square

Proposition 3.8. *The axes of primal and Christoffel dual orthogonal circles coincide. The axes are given by the face normals*

$$(12) \quad m : F(\mathcal{G}) \rightarrow \mathbb{R}^3, \quad f \mapsto m_f := c_f^* - c_f,$$

which connect centers of primal and Christoffel dual orthogonal circles, as shown in Figure 7.

Proof. The circles lie in parallel planes and they lie on a common sphere. This follows from the fact that the linear subspace containing the lift of a fundamental cmc hexahedron (as illustrated in Figure 7) to $\mathbb{R}^{4,1}$ is four-dimensional. Its orthogonal complement represents a sphere that is orthogonal to all eight vertex spheres and, in particular, contains the two circles. Consequently, their circle axes coincide and are given by m_f . \square

We use the geometric observations to prove Theorem 3.6.

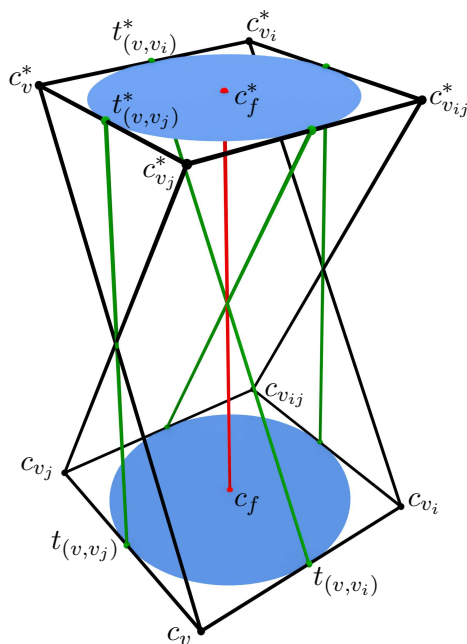


Figure 7. A fundamental hexahedron of an S_1 -cmc pair, formed by a pair of primal and Christoffel dual faces and corresponding vertex normals (black). The orthogonal face circles, shown in blue, touch the faces at the points $t_{(v,v')}$ and $t_{(v,v')}$. The edge normals, shown in green, connect these points on corresponding primal and dual edges. The face normal (red) connects the centers of primal and dual orthogonal circles and is orthogonal to both faces.

Proof of Theorem 3.6. The Gauss map (8) and the center nets c and c^* have parallel edges

$$(13) \quad c_v - c_{v'} \parallel n_v - n_{v'} \parallel c_v^* - c_{v'}^*.$$

In particular, the Gauss map shares the same face normals (12),

$$m_f \perp [n_v, n_{v_i}, n_{v_{ij}}, n_{v_j}],$$

and therefore is a Q-net. Using the squared length of the edge normals (11), we define two global constants:

$$\Delta_+^2 := -2\alpha + 2\lambda, \quad \Delta_-^2 := -2\alpha - 2\lambda.$$

The Gauss images of the edge normals (9) lie on two concentric spheres S_{\pm}^2 of radii Δ_{\pm} , as illustrated in Figure 8. A combination of (10) and (13) yields

$$l_{(v,v')} \perp n_v - n_{v'}.$$

Thus, the edges $n_v - n_{v'}$ are alternately tangent to S_+^2 and S_-^2 at the points $l_{(v,v')}$. By a suitable scaling of the initial S_1 -cmc pair, we can adjust Δ_+ and Δ_- to new radii r_+ and r_- that satisfy the relation $r_+ r_- = 1$. Consequently, the Gauss map (8) indeed forms a two-sphere Koebe net. \square

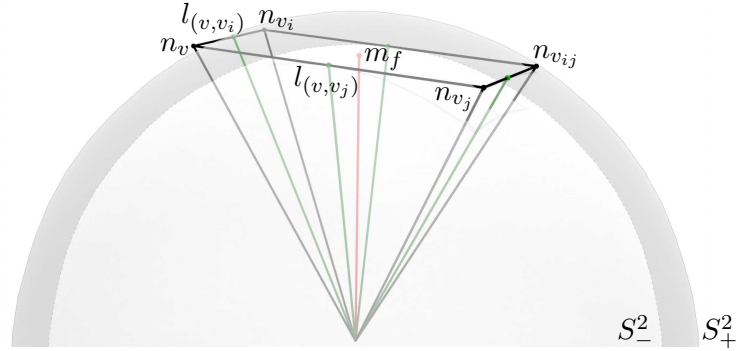


Figure 8. The Gauss image of the fundamental S_1 -cmc hexahedron of Figure 7, which forms a face of a two-sphere Koebe net. It alternately touches the two spheres S_+^2 and S_-^2 , with the points of tangency given by the edge normal vectors $l_{(v,v')} \in S_\pm^2$ (green). Horizontal edges always touch S_+^2 and vertical edges always touch S_-^2 . The vector m_f (red) is orthogonal to the planar face.

The edges of the Gauss map may change direction relative to the edges of c . From Figures 6 and 7, we can observe that the change in orientation can only occur along horizontal edges.

3.2. Discrete curvatures. We have seen that the center nets c and c^* of two S_1 -isothermic surfaces s and s^* and the Gauss map n are Q-nets with parallel edges. We interpret the pair (c, n) as a Q-net with a parallel Gauss map n . Discrete curvatures for such pairs were defined in [18] using a discrete version of the classical Steiner formula. Consider the one parameter family of parallel surfaces $c_t := c + tn$ for $t \in \mathbb{R}$. Let $c(f)$ and $n(f)$ be the quadrilaterals (with parallel edges) corresponding to the same combinatorial face f . The area of the quadrilateral $c_t(f)$ is a quadratic polynomial of t

$$A(c_t(f)) = (1 - 2H_f t + K_f t^2) A(c(f)),$$

where

$$(14) \quad H_f = -\frac{A(c(f), n(f))}{A(c(f))} \quad \text{and} \quad K_f = \frac{A(n(f))}{A(c(f))},$$

define *discrete mean curvature* and *discrete Gaussian curvature* of the face f , respectively. Recall that the area form of a planar polygon $A(P)$ is a quadratic form on the space of planar polygons. The corresponding symmetric bilinear form

$$A(P, Q) = \frac{1}{2}(A(P + Q) - A(P) - A(Q))$$

is the *mixed area* of two planar polygons P and Q with parallel edges.

In a slight misnomer we will now consider the mean curvature of a pair (s, n) of an S_1 -isothermic surface and its Gauss map, where we in fact consider the mean curvature of the pair (c, n) as discussed above.

Theorem 3.9. *Let s and s^* be an S_1 -cmc pair such that the Gauss map n , given by (8), forms a two-sphere Koebe net. Then the pair (s, n) has constant discrete mean curvature*

$H = 1$. The Christoffel dual is a constant vertex offset surface in normal direction at distance 1:

$$(15) \quad c^* = c + n.$$

Proof. Identity (15) is the definition of n . The mixed area vanishes for pairs of Christoffel dual quadrilaterals [18, 20]. Thus

$$A(c, c^*) = 0,$$

which is equivalent to

$$H = -\frac{A(c, n)}{A(c)} = 1$$

if $c^* = c + n$. □

We restrict our considerations to discrete $H = 1$ cmc surfaces. An S_1 -cmc surface pair may be scaled, $s_\mu = \mu s$, $s_\mu^* = \mu s^*$, by a global factor μ while maintaining the same Gauss map n , to obtain a pair (s_μ, n) with $H_\mu = \frac{1}{\mu}$. The center net c_μ^* is a normal offset surface of c_μ at distance $\frac{1}{H_\mu}$:

$$(16) \quad c_\mu^* = c_\mu + \frac{1}{H_\mu}n,$$

analogous to the smooth case.

4. TWO-SPHERE KOEBE NETS AND ORTHOGONAL RING PATTERNS IN THE SPHERE

In this section we will consider the correspondence between two-sphere Koebe nets and spherical orthogonal ring patterns detached from S_1 -cmc surfaces. Classical Koebe polyhedra are known to be in one to one correspondence with spherical orthogonal circle patterns. Each vertex of a Koebe polyhedron can be associated with a sphere centered at the vertex, which intersects the unit sphere S^2 orthogonally. The intersection of all such spheres with S^2 yields a circle packing. A second circle packing is obtained by intersecting the faces of the Koebe polyhedron with S^2 . These two families of circles together form an orthogonal circle pattern. Conversely, by lifting the circle centers of a circle pattern off the unit sphere, one can obtain a pair of combinatorially dual Koebe polyhedra [8].

Rather than treating primal and dual combinatorics separately, we will now consider the more general combinatorics of S-quad graphs.

Definition 4.1. An S-quad-graph is a quad graph \mathcal{S} with interior vertices of even degree and the following additional properties:

- (i) The 1-skeleton of \mathcal{S} is bipartite and the vertices are bi-colored black and white

$$V(\mathcal{S}) = V_w(\mathcal{S}) \dot{\cup} V_b(\mathcal{S}).$$

Then each quadrilateral has two black vertices and two white vertices.

- (ii) The white vertices may be labeled \textcircled{C} and \textcircled{S} ,

$$V_w(\mathcal{S}) = V_{\textcircled{S}}(\mathcal{S}) \dot{\cup} V_{\textcircled{C}}(\mathcal{S}),$$

in such a way that each quadrilateral has one white vertex labeled \textcircled{C} and one white vertex labeled \textcircled{S} .

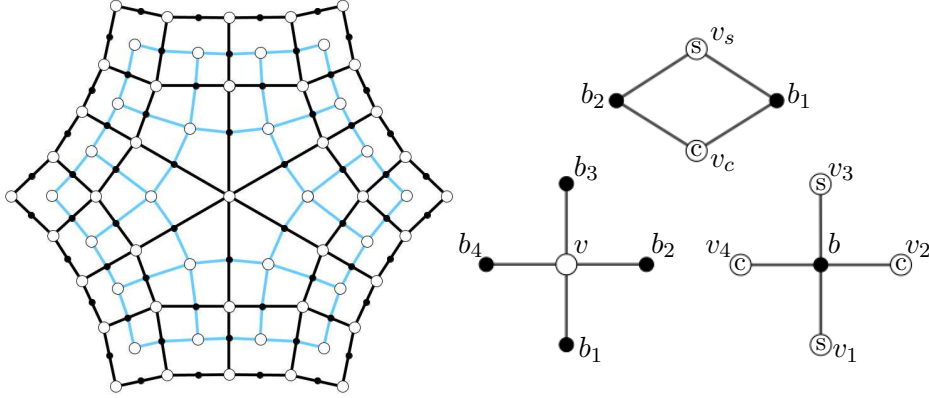


Figure 9. Left: The two graphs \mathcal{G} (black, consisting of white \textcircled{S} -vertices) and \mathcal{G}^* (blue, consisting of white \textcircled{C} -vertices) associated to an S-quad graph \mathcal{S} . From a graph \mathcal{G} one obtains the S-quad graph via central extension, i.e., by introducing a new white vertex per face and a new black vertex per edge. Right: Labeling of vertices.

(iii) Interior black vertices and interior \textcircled{C} -vertices have degree 4.

Recall that for S-isothermic surfaces, we considered quad graphs with interior vertices of even degree. Any graph \mathcal{G} of this type can be extended to an S-quad graph via *central extension*, see Figure 9. Conversely, from any S-quad graph \mathcal{S} , one can obtain two graphs: a quad graph \mathcal{G} with interior vertices of even degree and its dual graph \mathcal{G}^* . The edge coloring of the graph \mathcal{G} into horizontal and vertical edges in Figure 2 can be consistently extended to \mathcal{S} so that all faces of \mathcal{S} have alternating horizontal and vertical edges.

Our definition of S-quad graphs is slightly more restrictive than the definition in [15], where neither of the graphs \mathcal{G} and \mathcal{G}^* is restricted to be a quad graph.

The Definition 3.5 of two spheres Koebe nets with underlying quad graph \mathcal{G} can be extended to graphs of the combinatorics of \mathcal{G}^* in a straightforward manner.

Definition 4.2. Let \mathcal{G} and \mathcal{G}^* be the two graphs associated with an S-quad graph \mathcal{S} . We call the two-sphere Koebe nets $k^s : V(\mathcal{G}) \rightarrow \mathbb{R}^3$ and $k^c : V(\mathcal{G}^*) \rightarrow \mathbb{R}^3$ a pair of dual two-sphere Koebe nets if they satisfy the following conditions:

- (1) The nets k^s and k^c touch the same two spheres S_+^2 and S_-^2 .
- (2) Vertex vectors of k^s form normals of the corresponding faces of k^c and vice versa.
- (3) Dual edges of k^s and k^c are orthogonal. Their points of tangency lie on different spheres and are projected to the same point on the unit sphere.

Pairs of dual two-sphere Koebe nets are examples of principle binets, which are pairs of combinatorially dual, conjugate nets with orthogonal dual edges. Principle binets were introduced in [5] as a discretization of a curvature line parametrization.

Let k^s and k^c be a pair of dual two-sphere Koebe nets. For our purposes, we assume that the points of tangency adjacent to a vertex of k^c or k^s , corresponding to the points b_1, b_2, b_3, b_4 in Figure 9 (right), are cyclically ordered, either in clockwise or in counter-clockwise order. We call the corresponding two-sphere Koebe nets *regular*. Note that the two-sphere Koebe nets obtained as the Gauss map from S_1 -cmc surfaces are regular. We

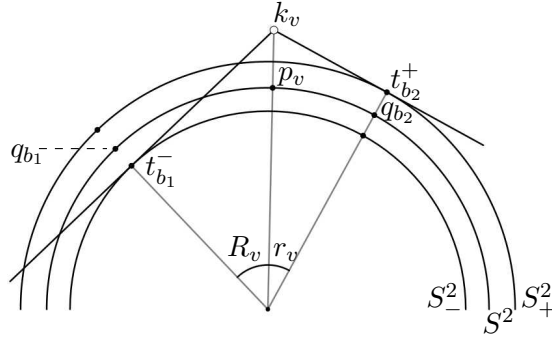


Figure 10. A vertex k_v of a two-sphere Koebe net, two adjacent edges with tangent points $t_{b_1}^-$ and $t_{b_2}^+$, and the projections p_v, q_{b_1} , and q_{b_2} onto S^2 . The corresponding ring (p_v, r_v, R_v) in the projection has center p_v , passes through q_{b_1} and q_{b_2} , and has spherical radii r_v and R_v given by the angles shown in the figure.

assume that the coloring of the edges of \mathcal{G} is chosen so that the horizontal edges touch S^2_+ and the vertical edges touch S^2_- .

For a white vertex $v \in V_w(\mathcal{S})$, let k_v denote the corresponding vertex of either k^s or k^c , and

$$(17) \quad p_v := \frac{k_v}{\|k_v\|}$$

its projection onto S^2 . For a black vertex $b \in V_b(\mathcal{S})$ there are two corresponding points of tangency, t_b^+ and t_b^- , one of which belongs to k^s , the other to k^c . By definition they lie on different spheres S^2_+ and S^2_- and project to the same point on S^2 :

$$(18) \quad q_b := \frac{t_b^+}{r^+} = \frac{t_b^-}{r^-},$$

where r_+ and r_- are the radii of S^2_+ and S^2_- , respectively. We will show that the projections (17) and (18) give rise to spherical rings (pairs of concentric circles) which intersect orthogonally [11]. For an illustration see Figure 10.

A ring is given by a triple (p, r, R) where $p \in S^2$ is the center of the ring, and r and R are the radii of the inner and the outer circles, respectively. We assign an orientation to the ring by allowing r to be negative: positive radius corresponds to counterclockwise orientation and negative radius corresponds to clockwise orientation. The outer radius is always positive. The spherical radii r and R are not allowed to be greater than $\frac{\pi}{2}$.

Definition 4.3. *Let \mathcal{S} be an S -quad graph. An orthogonal ring pattern consists of rings associated with the white vertices of \mathcal{S} that satisfy the following properties:*

- (1) *The rings associated with the \odot and the \ominus vertex of a quad, $(p_{v_1}, r_{v_1}, R_{v_1})$ and $(p_{v_2}, r_{v_2}, R_{v_2})$, intersect orthogonally, i. e. the larger circle of one ring intersects the smaller circle of the other ring orthogonally, and vice versa.*
- (2) *For four rings $(p_{v_1}, r_{v_1}, R_{v_1})$, $(p_{v_2}, r_{v_2}, R_{v_2})$, $(p_{v_3}, r_{v_3}, R_{v_3})$ and $(p_{v_4}, r_{v_4}, R_{v_4})$ adjacent to a black vertex b and ordered according to the combinatorics of the quad graph, see Figure 9 (right), the inner circles (p_{v_1}, r_{v_1}) and (p_{v_3}, r_{v_3}) and the outer circles (p_{v_2}, R_{v_2}) and (p_{v_4}, R_{v_4}) pass through one point. (Then orthogonality implies that the two inner and the two outer circles touch at this point.)*

- (3) The black vertices of the S -quad graph correspond to the touching points. For each ring, these points are ordered according to the orientation of the ring, i.e., the points corresponding to b_1, b_2, b_3, b_4 in Figure 9 (right) are ordered counterclockwise if the ring corresponding to the white vertex v is positively oriented, $r_v > 0$, and clockwise if $r_v < 0$.

Proposition 4.4. The projections p_v and q_b , given in (17) and (18), of vertices and tangent points of pairs of dual two-sphere Koebe nets define spherical rings (p_v, r_v, R_v) that are centered at p_v and pass through the projections q_b of adjacent tangent points. The spherical radii r_v and R_v are given (up to sign) by

$$(19) \quad \cos(r_v) = \frac{r_+}{\|k_v\|}, \cos(R_v) = \frac{r_-}{\|k_v\|}.$$

For regular two-sphere Koebe nets, the rings form a spherical orthogonal ring pattern, see Figure 12.

Proof. All tangent points on S^2_+ adjacent to a vertex k_v have the same distance to k_v and are therefore projected onto a circle in S^2 centered at p_v . The same holds for the tangent points on S^2_- , see Figure 11 (1). The two circles form a spherical ring (p_v, r_v, R_v) , where for the radii r_v and R_v we have (19), since they coincide with the angles shown in Figure 10.

Now let v_c, b_1, v_s, b_2 be the vertices of a face of \mathcal{S} , see Figure 9 (right). The two corresponding rings in the projection, $(p_{v_s}, r_{v_s}, R_{v_s})$ and $(p_{v_c}, r_{v_c}, R_{v_c})$, intersect orthogonally.

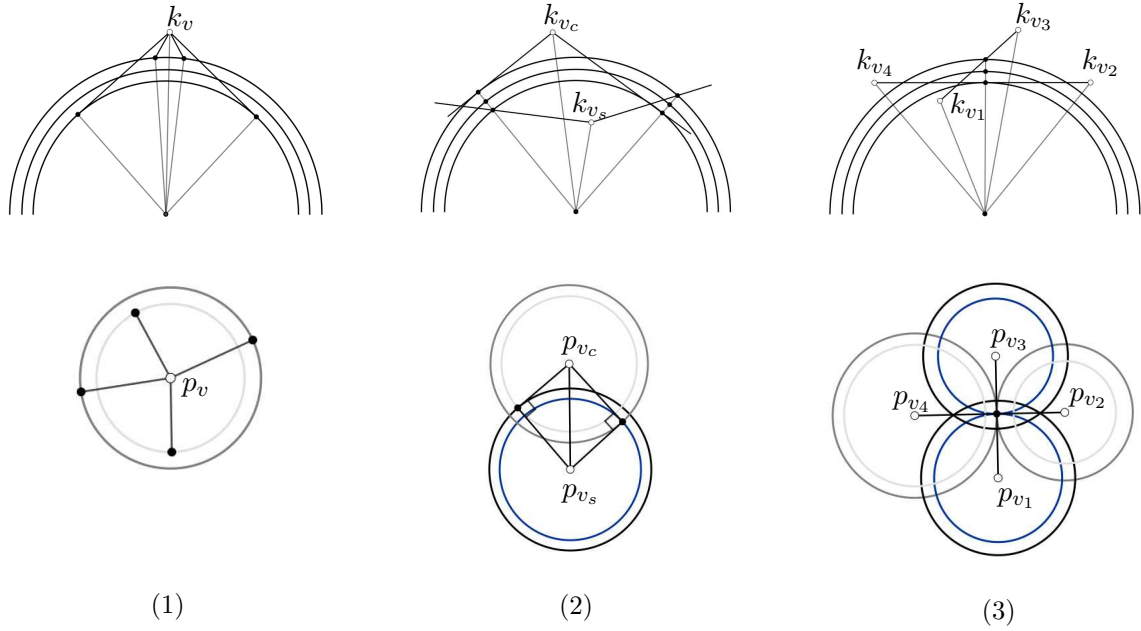


Figure 11. Projecting a pair of dual two-sphere Koebe nets to S^2 . (1) Vertices and adjacent tangent points project to spherical rings, (2) neighboring rings intersect orthogonally, (3) rings of white vertices adjacent to a common black vertex pass through a common point.

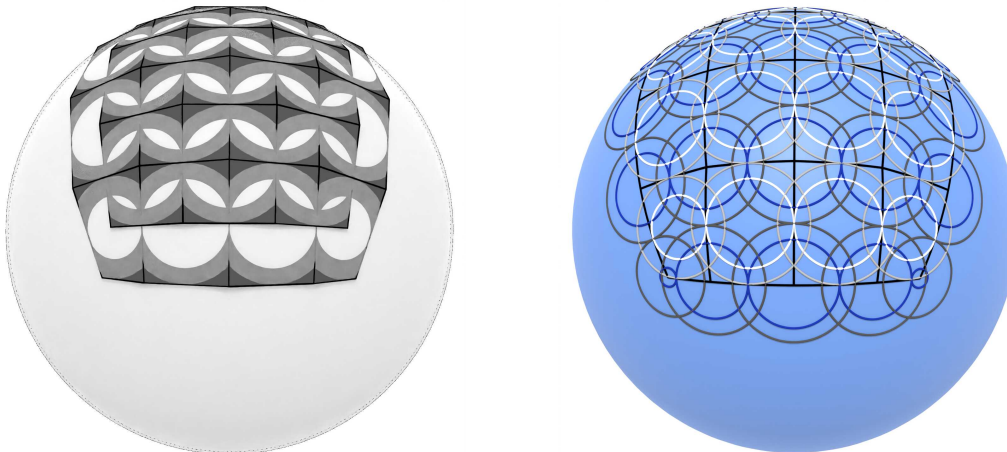


Figure 12. A pair of dual two-sphere Koebe nets (left) and the corresponding spherical orthogonal ring pattern (shown with the combinatorics of \mathcal{G} , right). Vertices of the two-sphere Koebe nets correspond to centers of spherical rings and points of tangency correspond to the touching points of rings.

To see this, we first note that tangent points on S^2_+ always project onto inner circles and tangent points on S^2_- always project onto outer circles. The orthogonality of the rings then follows from the orthogonality of pairs of dual edges of the two-sphere Koebe nets, see Figure 11 (2).

With these observations we also find, that four rings corresponding to four vertices v_1, v_2, v_3, v_4 adjacent to a common black vertex b , see Figure 9 (right), pass through a common point q_b , see Figure 11 (3). Finally, the regularity assumption allows to choose signs of the inner radii of the rings such that the rings are oriented according to the order of the adjacent touching points, and indeed form a spherical orthogonal ring pattern. \square

If two spherical rings, (p_v, r_v, R_v) and $(p_{v'}, r_{v'}, R_{v'})$, intersect orthogonally, then applying the spherical Pythagorean theorem, we obtain

$$\frac{\cos(R_v)}{\cos(r_v)} = \frac{\cos(R_{v'})}{\cos(r_{v'})}.$$

For spherical orthogonal ring patterns, this implies that there exists a global constant $q < 1$ such that the radii of the inner and outer circles of all rings are related by

$$(20) \quad q \cos r_v = \cos R_v.$$

There are two distinct directions in an orthogonal ring pattern, corresponding to horizontal and vertical edges of \mathcal{S} . Along horizontal edges, the inner circles of next neighboring rings touch, along vertical edges the outer circles of next neighboring rings touch. The rings form two families, corresponding to the coloring of white vertices $V_w(\mathcal{S})$ into white \textcircled{S} -vertices and white \textcircled{C} -vertices. Touching rings always belong to the same family. Recall that the radius of inner circles can be negative, which can cause the ring pattern to flip and reverse direction along horizontal edges, see Figure 1 for an example.

A pair of dual two-sphere Koebe nets can be uniquely recovered from the corresponding spherical orthogonal ring pattern.

Proposition 4.5. *Consider a spherical orthogonal ring pattern with rings (p_v, r_v, R_v) and global parameter $q < 1$. Define the vertices*

$$(21) \quad k_v := \frac{\sqrt{q}}{\cos(R_v)} p_v = \frac{1}{\sqrt{q} \cos(r_v)} p_v$$

and the points

$$(22) \quad t_b^+ := \frac{1}{\sqrt{q}} q_b, \quad t_b^- := \sqrt{q} q_b,$$

which scale the centers p_v and the touching points q_b off the unit sphere. By restricting the map

$$k : V_w(\mathcal{S}) \rightarrow \mathbb{R}^3, \quad v \mapsto k_v$$

to the graphs \mathcal{G} and \mathcal{G}^* of \mathcal{S} , one obtains a pair of regular, dual two-sphere Koebe nets, which are alternately tangent to the two spheres S_+^2 and S_-^2 , with radii $\frac{1}{\sqrt{q}}$ and \sqrt{q} , at the points (22).

Proof. Consider four vertices v_1, v_2, v_3, v_4 adjacent to a common black vertex b in \mathcal{S} , see Figure 9 (right). The corresponding spherical rings $(p_{v_1}, r_{v_1}, R_{v_1})$, $(p_{v_2}, r_{v_2}, R_{v_2})$, $(p_{v_3}, r_{v_3}, R_{v_3})$ and $(p_{v_4}, r_{v_4}, R_{v_4})$ pass through a common point q_b . Suppose that the inner circles of $(p_{v_1}, r_{v_1}, R_{v_1})$ and $(p_{v_3}, r_{v_3}, R_{v_3})$ and the outer circles of $(p_{v_2}, r_{v_2}, R_{v_2})$ and $(p_{v_4}, r_{v_4}, R_{v_4})$ touch in q_b , see Figure 11 (3). Scaling the centers and the touching points by (21) and (22) we obtain the edges $[k_{v_1}, k_{v_3}]$ and $[k_{v_2}, k_{v_4}]$ such that

$$(23) \quad t_b^+ \in [k_{v_1}, k_{v_3}], \quad q_b \perp [k_{v_1}, k_{v_3}], \quad t_b^- \in [k_{v_2}, k_{v_4}], \quad q_b \perp [k_{v_2}, k_{v_4}].$$

The orthogonality of neighboring rings and the tangency of next neighboring rings implies the orthogonality

$$(24) \quad [k_{v_1}, k_{v_3}] \perp [k_{v_2}, k_{v_4}].$$

It remains to show that for the two resulting polyhedral surfaces the vertex vectors of one surface form the face normal vectors of the other. To this end consider a face of \mathcal{G} with white (S) -vertices $v_{s_1}, v_{s_2}, v_{s_3}, v_{s_4}$ dual to a vertex v_c . The vector k_{v_c} is orthogonal to all four edges of the quadrilateral $[k_{v_{s_1}}, k_{v_{s_2}}, k_{v_{s_3}}, k_{v_{s_4}}]$, which in particular implies in particular the planarity of this quadrilateral. To show, for example the orthogonality

$$(25) \quad [k_{v_{s_1}}, k_{v_{s_2}}] \perp k_{v_c}$$

we observe that

$$(26) \quad [k_{v_{s_1}}, k_{v_{s_2}}] \perp [t_b^-, k_{v_c}].$$

The latter orthogonality follows from (24) and the fact that $t_b^- \in [k_{v_c}, k_{v_c'}]$. A combination of (23) and (26) implies (25). The same also holds for faces of \mathcal{G}^* with valency greater than four. \square

We have established the following correspondence, shown in Figure 12.

Theorem 4.6. *Pairs of regular, dual two-sphere Koebe nets touching the spheres S_+^2 and S_-^2 , with radii r_+ and r_- , are in one to one correspondence with orthogonal ring patterns in S^2 with global parameter $q = \frac{r_-}{r_+}$. Vertices of the Koebe nets correspond to centers of spherical rings, while points of tangency of the Koebe nets correspond to touching points of the rings.*

Remark. Classical Koebe nets are specific examples of S_1 -isothermic surfaces. In this case, the vertex spheres are given by the spheres that intersect S^2 orthogonally, as discussed earlier in this section. However, for two-sphere Koebe nets, each vertex has a pair of concentric vertex spheres: the smaller sphere intersects S_+^2 orthogonally and the larger sphere intersects S_-^2 orthogonally. The smaller spheres touch along horizontal edges, while the larger spheres touch along vertical edges. For both families of vertex spheres, orthogonal face circles exist, formed by the intersection of the two-sphere Koebe net with the spheres S_+^2 and S_-^2 , respectively. Unlike classical Koebe nets, two-sphere Koebe nets do not belong to the class of S_1 -isothermic surfaces.

5. ANALYTIC DESCRIPTION OF ORTHOGONAL RING PATTERNS IN THE SPHERE

This section presents the basics of the analytic description, including the variational description, of spherical orthogonal ring patterns. For proofs and further details we refer to [11].

We consider an S-quad graph \mathcal{S}_z that is defined by a simply connected subset of squares of the \mathbb{Z}^2 lattice in \mathbb{R}^2 . Our main example is a combinatorial rectangle

$$(27) \quad \mathcal{S}_z = \{(i, j) \in \mathbb{Z}^2 \mid 1 \leq i \leq I, 1 \leq j \leq J\}.$$

Let us now consider an orthogonal ring pattern with global parameter $q \leq 1$ and underlying S-quad graph \mathcal{S}_z . There is a ring associated with each white vertex, with inner radius r_v and outer radius $R_v \leq \frac{\pi}{2}$. Due to (20), these radii can be uniformized in terms of Jacobi elliptic functions,

$$(28) \quad \cos r_v = \operatorname{sn}(\beta_v, q), \quad \sin r_v = \operatorname{cn}(\beta_v, q), \quad \sin R_v = \operatorname{dn}(\beta_v, q),$$

associating a variable $\beta_v \in [0, 2K]$ to each ring. Here K denotes the real quarter period of Jacobi elliptic functions [44].

To characterize rings forming orthogonal ring patterns, let us introduce the function

$$(29) \quad g(x) := \frac{\pi}{2} - \arg \operatorname{sn} \left(\frac{x + iK'}{2} \right).$$

The uniformizing variables $\beta : V_w(\mathcal{S}_z) \rightarrow [0, 2K]$ determine an orthogonal ring pattern with $R \leq \frac{\pi}{2}$ if and only if for all internal white vertices v they satisfy

$$\sum_{v' \sim v} g(\beta_v + \beta_{v'}) - g(\beta_v - \beta_{v'}) = 2\pi,$$

where the sum is taken over all neighboring rings of (p_v, r_v, R_v) that intersect it orthogonally. Combinatorially, neighboring vertices $v' \sim v$ are the two white vertices of an elementary quad of the S-quad graph \mathcal{S}_z , see Figure 9 (right). With prescribed nominal

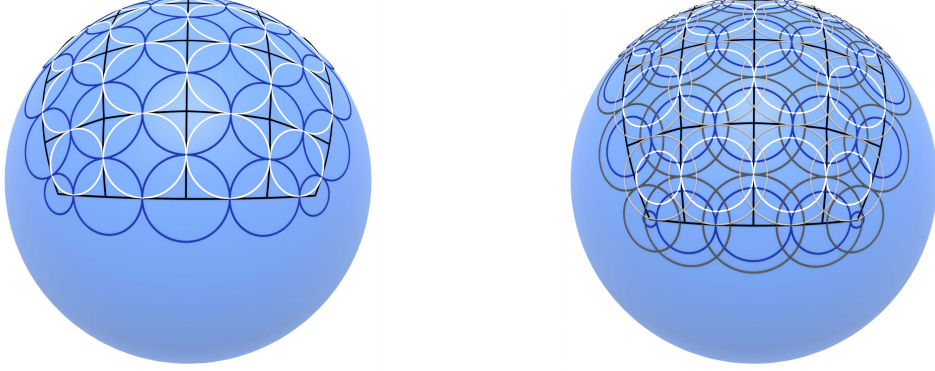


Figure 13. A local patch of a spherical orthogonal circle pattern with $q=0.999999$ (left) and its deformation to a spherical orthogonal ring pattern with $q=0.99$ (right). All corner angles are of size $\frac{2\pi}{3}$.

angles Θ , a similar condition must hold for white boundary vertices:

$$\begin{aligned} \pi \deg(v) + \sum_{v' \sim v} g(\beta_v - \beta_{v'}) - g(\beta_v + \beta_{v'}) &= \Theta_v, \quad \text{if } r_v > 0, \\ \sum_{v' \sim v} g(\beta_v - \beta_{v'}) - g(\beta_v + \beta_{v'}) &= \Theta_v, \quad \text{if } r_v < 0. \end{aligned}$$

Using the anti-derivative of (29),

$$(30) \quad F(x) = \int_0^x \frac{\pi}{2} - \arg \operatorname{sn} \frac{u + iK'}{2} du = \int_0^x \arctan \frac{(1+q) \operatorname{sn} \frac{u}{2}}{\operatorname{cn} \frac{u}{2} \operatorname{dn} \frac{u}{2}} du,$$

one defines the functional

$$(31) \quad S_{sph}(\beta) := \sum_{(v,v')} (F(\beta_v - \beta_{v'}) - F(\beta_v + \beta_{v'})) + \sum_v \Phi_v \beta_v,$$

where the first sum is taken over all pairs of white vertices corresponding to neighboring rings and the second sum over all white vertices $v \in V_w(\mathcal{S}_z)$. Φ_v are some prescribed parameters at the vertices.

Theorem 5.1. *The critical points β of the functional S_{sph} with all $\beta_v \in [0, 2K]$ and*

$$\begin{aligned} \Phi_v &= 2\pi && \text{for inner rings,} \\ \Phi_v &= \pi \deg(v) - \Theta_v && \text{for positively oriented boundary rings,} \\ \Phi_v &= -\Theta_v && \text{for negatively oriented boundary rings,} \end{aligned}$$

correspond to spherical orthogonal ring patterns with all $R_v \leq \frac{\pi}{2}$. Here Θ_v is the nominal angle covered by the neighboring rings respectively.

A proof of the theorem is provided in [11]. The functional (31) is not convex, its second derivative

$$\begin{aligned} D^2 S_{sph} &= \frac{1}{2} \sum_{(v,v')} (\operatorname{dn}(\beta_v - \beta_{v'}) + q \operatorname{cn}(\beta_v - \beta_{v'})) (d\beta_v - d\beta_{v'})^2 - \\ &\quad (\operatorname{dn}(\beta_v + \beta_{v'}) + q \operatorname{cn}(\beta_v + \beta_{v'})) (d\beta_v + d\beta_{v'})^2 \end{aligned}$$

is negative for the tangent vector $u = \sum_v \partial/\partial\beta_v$, the index is therefore at least 1. We define a reduced functional $\tilde{S}_{sph}(\beta)$ by maximizing in the direction u :

$$(32) \quad \tilde{S}_{sph}(\beta) = \max_t S_{sph}(\beta + tu).$$

Obviously, $\tilde{S}_{sph}(\beta)$ is invariant under translations in the direction u . Now the idea is to minimize $\tilde{S}_{sph}(\beta)$ restricted to $\sum_v \beta_v = 0$. This method has proven to be amazingly powerful for our computations. In particular, it was used to produce branched orthogonal ring patterns in the sphere and the examples in Section 8.

For $q = 1$ the two radii, R_v and r_v , of a ring coincide and we obtain spherical orthogonal circle patterns. The spherical radii of circles can also be expressed using β -variables, which we denote by β^0 , related in the following way

$$\tanh \beta_v^0 = \cos R_v, \quad \frac{1}{\cosh \beta_v^0} = \sin R_v.$$

The corresponding variation principle for orthogonal circle patterns was suggested in [51] and used in [15]. The global existence and uniqueness of spherical orthogonal circle pattern for a given polytopal cell decomposition of the sphere is ensured by Koebe's Theorem, see e.g. [15].

Factorizing a reflectionally symmetric cell decomposition by its symmetry groups one obtains existence and uniqueness results for circle patterns on the corresponding factor. Further, solutions β^0 of a Dirichlet or Neumann boundary value problem for circle patterns (corresponding to $q = 1$) allow small deformations to orthogonal ring patterns with the same combinatorial and boundary data (corresponding to $q = 1 - \epsilon$ for small ϵ). In [11] this fact was proven for rigid circle patterns, i.e., the ones with a non-degenerate Hessian

$$(33) \quad \det \left(\frac{\partial^2 S_{sph}}{\partial \beta_v^0 \partial \beta_{v'}^0} \right) \neq 0.$$

An example is shown in Figure 13.

We will use this deformation of circle patterns to ring patterns in Section 7 to construct discrete cmc surfaces with small mean curvature as deformations of discrete minimal surfaces.

6. CONSTRUCTING CMC SURFACES IN \mathbb{R}^3

How does one construct a discrete S_1 -cmc surface analogous to a particular continuous cmc surface under investigation? In this section we outline the general method for doing so. An analogous construction scheme for discrete S_1 -minimal surfaces is described in [15]. Figure 14 illustrates the construction of a discrete Schwarz P cmc surface. The difficult part here is to construct the ring pattern corresponding to the combinatorics of curvature lines and boundary conditions, obtained from the smooth surface (paragraphs 1 and 2 below). The remaining steps, constructing the two-sphere Koebe net and the corresponding pair of S_1 -cmc surfaces (paragraphs 3 and 4) are rather direct. Note that we only consider simply connected domains.

1. Investigate the Gauss image of the curvature lines.

The Gauss map of the continuous cmc surface maps its curvature lines onto the sphere. We start with a qualitative picture of this image, which is a quad graph immersed in the

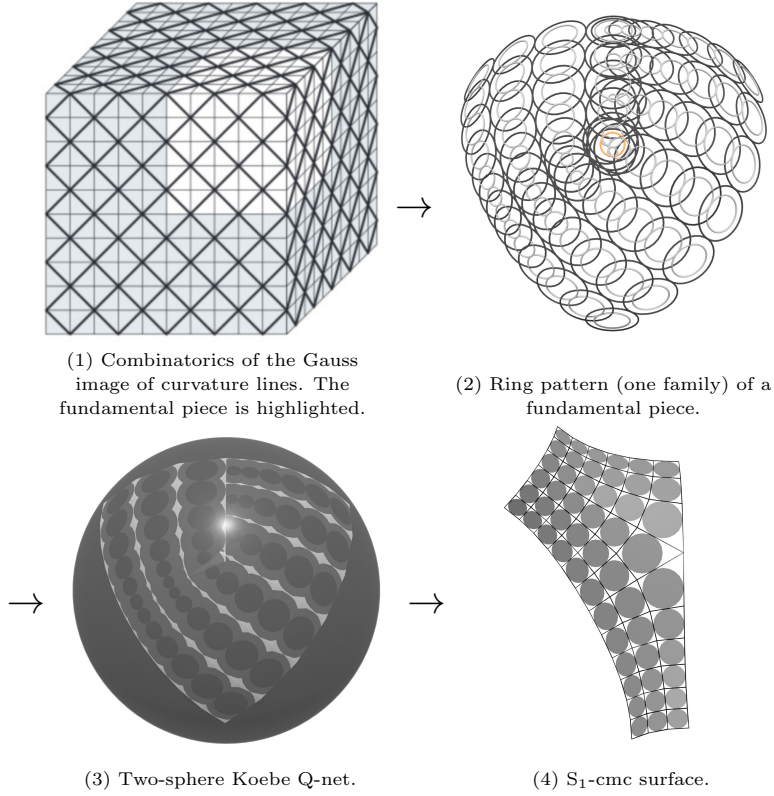


Figure 14. Construction of a discrete S_1 -cmc Schwarz P surface.

sphere. Here the choice of number of curvature lines corresponds to a choice of different levels of refinement of the discrete surface. Umbilics must be white vertices. Generically, the interior vertices are of degree four. Exceptional vertices correspond to ends and umbilic points of the continuous cmc surface. For example, in Figure 14 (1), the corners of the cube are exceptional.

2. Construct the ring pattern.

Next, from the quad graph, a parameter q , and boundary conditions, we construct a ring pattern by solving the corresponding boundary value problem. For suitable initial data, minimizing the reduced functional (32) determines the corresponding ring pattern. White vertices correspond to centers of rings, black vertices to touching points. Figure 14 (2) shows the ring pattern around an umbilic point. Note that in this example, the Gauss map forms a double covering of the sphere, of which only one layer is shown in the figure.

3. Construct the dual two-sphere Koebe nets.

Now we construct the pair of dual two-sphere Koebe nets from the ring pattern. The white vertices labeled by \textcircled{S} and \textcircled{C} correspond to the vertices of a pair of dual two-sphere Koebe nets k^s and k^c . These vertices correspond to the spheres and the orthogonal circles of the S_1 -cmc surface, respectively.

4. Construct the discrete S_1 -cmc surface from its Gauss map.

In Theorem 3.6 we described how an S_1 -cmc pair generates a two-sphere Koebe net as its

Gauss map. Here we reverse this construction and show how to recover an S_1 -cmc pair from its Gauss map. The essential part of this construction is to determine the radii of vertex spheres and face circles for the surfaces in terms of data from the ring pattern, or the Koebe nets. To determine these radii we will consider the central extension of a two-sphere Koebe net k^s , i.e., the map $k_{\boxplus} : V(\mathcal{S}) \rightarrow \mathbb{R}^3$, such that

$$(34) \quad \begin{aligned} V_{\textcircled{S}} \ni v_s &\mapsto \text{vertices } k_{v_s} \text{ of } k^s; \\ V_{\textcircled{C}} \ni v_c &\mapsto \text{face centers } \tilde{k}_{v_c} \text{ of } k^s; \\ V_b \ni b &\mapsto \text{tangent points } t_b^\pm \text{ of } k^s; \end{aligned}$$

see Figure 15 (left). The center \tilde{k}_{v_c} of a face $[k_{v_{s_1}}, k_{v_{s_2}}, k_{v_{s_3}}, k_{v_{s_4}}]$ is the *properly scaled* dual vector, i.e.

$$(35) \quad \tilde{k}_{v_c} \perp [k_{v_{s_1}}, k_{v_{s_2}}, k_{v_{s_3}}, k_{v_{s_4}}], \quad \tilde{k}_{v_c} \in [k_{v_{s_1}}, k_{v_{s_2}}, k_{v_{s_3}}, k_{v_{s_4}}].$$

Consider a fundamental piece $[k_{v_s}, t_b^-, \tilde{k}_{v_c}, t_b^+]$ of k_{\boxplus} , consisting of one vertex, one face center and two touching points. In this section we consider the case shown in Figure 15 (left), when this quadrilateral is embedded. Its edge lengths can be expressed in terms of the radii of the corresponding orthogonal ring pattern, see Figure 10,

$$(36) \quad \begin{aligned} \|t_b^- - k_{v_s}\| &= \sqrt{q} \tan(R_{v_s}), & \|\tilde{k}_{v_c} - t_b^-\| &= \sqrt{q} \sin(r_{v_c}), \\ \|t_b^+ - \tilde{k}_{v_c}\| &= \frac{1}{\sqrt{q}} \sin(R_{v_c}), & \|k_{v_s} - t_b^+\| &= \frac{1}{\sqrt{q}} \tan(r_{v_s}). \end{aligned}$$

Note that the embeddedness of the quadrilateral corresponds to $r_{v_c} > 0$ and $r_{v_s} > 0$. If the two-sphere Koebe net is the Gauss map of an S_1 -cmc pair then the lengths (36) are related to the vertex sphere radii $d_{v_s}, d_{v_s}^*$ and the face circle radii $d_{v_c}, d_{v_c}^*$ of the S_1 -cmc pair such that

$$(37) \quad \begin{aligned} \|t_b^- - k_{v_s}\| &= d_{v_s} + d_{v_s}^*, & \|\tilde{k}_{v_c} - t_b^-\| &= d_{v_c} - d_{v_c}^*, \\ \|t_b^+ - \tilde{k}_{v_c}\| &= d_{v_c} + d_{v_c}^*, & \|k_{v_s} - t_b^+\| &= d_{v_s} - d_{v_s}^*, \end{aligned}$$

see Figure 15 (right). Here we use the parallelity of the primal and dual edges. A combination of (36) and (37) uniquely determines the radii of vertex spheres and face circles:

$$(38) \quad \begin{aligned} d_{v_s} &= \frac{1}{2}(\sqrt{q} \tan R_{v_s} + \frac{1}{\sqrt{q}} \tan r_{v_s}), & d_{v_c} &= \frac{1}{2}(\frac{1}{\sqrt{q}} \sin R_{v_c} + \sqrt{q} \sin r_{v_c}) \\ d_{v_s}^* &= \frac{1}{2}(\sqrt{q} \tan R_{v_s} - \frac{1}{\sqrt{q}} \tan r_{v_s}), & d_{v_c}^* &= \frac{1}{2}(\frac{1}{\sqrt{q}} \sin R_{v_c} - \sqrt{q} \sin r_{v_c}). \end{aligned}$$

Equivalently, in terms of the β -variables (28) the identities (36) can be expressed as

$$(39) \quad \begin{aligned} \|t_b^- - k_{v_s}\| &= \frac{1}{\sqrt{q}} \frac{\text{dn } \beta_{v_s}}{\text{sn } \beta_{v_s}}, & \|\tilde{k}_{v_c} - t_b^-\| &= \sqrt{q} \text{cn } \beta_{v_c}, \\ \|t_b^+ - \tilde{k}_{v_c}\| &= \frac{1}{\sqrt{q}} \text{dn } \beta_{v_c}, & \|k_{v_s} - t_b^+\| &= \frac{1}{\sqrt{q}} \frac{\text{cn } \beta_{v_s}}{\text{sn } \beta_{v_s}}. \end{aligned}$$

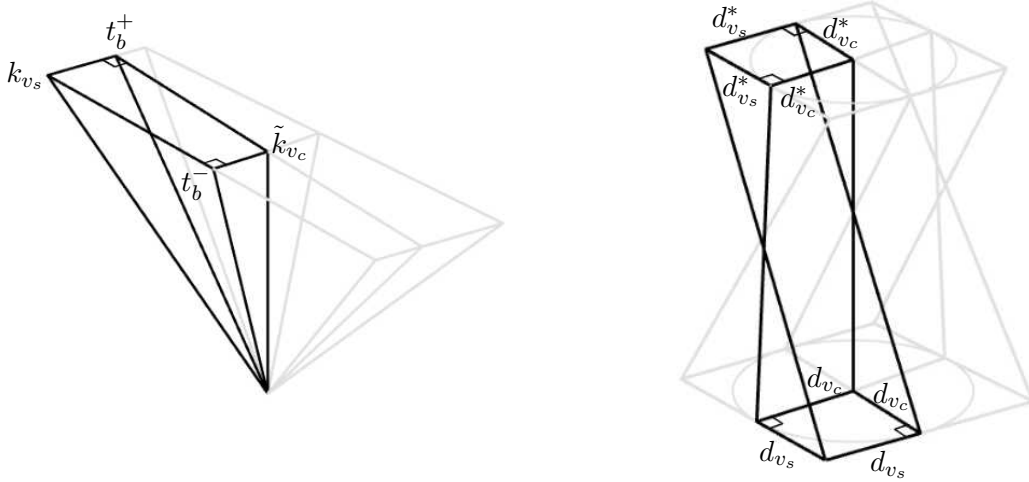


Figure 15. Left: A fundamental piece of a two-sphere Koebe net with a pair of opposite right angles. Right: Corresponding primal and dual fundamental kites and their normal vectors in a fundamental S_1 -cmc hexahedron. The labels denote the radii of the vertex spheres, d_{v_s} and $d_{v_s}^*$, and the radii of the face circles, d_{v_c} and $d_{v_c}^*$.

The radii (38) become

$$(40) \quad \begin{aligned} d_{v_s} &= \frac{1}{2} \frac{1}{\sqrt{q}} \left(\frac{\operatorname{dn} \beta_{v_s} + \operatorname{cn} \beta_{v_s}}{\operatorname{sn} \beta_{v_s}} \right), & d_{v_c} &= \frac{1}{2} \frac{1}{\sqrt{q}} (\operatorname{dn} \beta_{v_c} + q \operatorname{cn} \beta_{v_c}), \\ d_{v_s}^* &= \frac{1}{2} \frac{1}{\sqrt{q}} \left(\frac{\operatorname{dn} \beta_{v_s} - \operatorname{cn} \beta_{v_s}}{\operatorname{sn} \beta_{v_s}} \right), & d_{v_c}^* &= \frac{1}{2} \frac{1}{\sqrt{q}} (\operatorname{dn} \beta_{v_c} - q \operatorname{cn} \beta_{v_c}). \end{aligned}$$

We denote these radii by d_v and d_v^* , where the choice $v \in V_{\mathbb{S}}$ or $v \in V_{\mathbb{C}}$ determines whether we are considering the vertex sphere radii or the face circle radii.

The identities (40) determine the length of all edges of the (central extension of the) S_1 -cmc pair. The directions are determined by the edge parallelism to the two-sphere Koebe net. The following theorem ensures that the resulting surfaces with these edge lengths and directions exist.

Theorem 6.1. *Let $k_{\boxplus} : V(\mathcal{S}) \rightarrow \mathbb{R}^3$ be the central extension (34) of a two-sphere Koebe net. Then the \mathbb{R}^3 -valued discrete one-form ∂c_{\boxplus} defined by*

$$(41) \quad \partial_{(v,b)} c_{\boxplus} = d_v \frac{\partial_{(v,b)} k_{\boxplus}}{\|\partial_{(v,b)} k_{\boxplus}\|},$$

and the \mathbb{R}^3 -valued discrete one-form ∂c_{\boxplus}^* defined by

$$(42) \quad \partial_{(v,b)} c_{\boxplus}^* = \pm d_v^* \frac{\partial_{(v,b)} k_{\boxplus}}{\|\partial_{(v,b)} k_{\boxplus}\|},$$

with d_v, d_v^* given by (40), are exact. The signs (+) and (−) in (42) are chosen for horizontal and vertical edges, respectively. The integration of (41) and (42) defines the central extension of two surfaces c and c^* , which, when appropriately placed, form the center nets of an S_1 -cmc pair s, s^* with the Gauss map k_{\boxplus} . The vertex sphere radii and face circle

radii of s and s^* are given by (40). The S_1 -cmc pair with the Gauss map k_{\boxplus} is unique up to translation.

Proof. We give a proof for the case of embedded quadrilaterals, see Figure 15 (left). The cases of non-embedded quadrilaterals, when $r_{v_c} < 0$ or $r_{v_s} < 0$, can be considered similarly, formulas (40), (41), (42) hold in these cases as well.

With (39) and by defining unit normal vectors u_1, u_2, u_3, u_4 in counterclockwise order along the edges of a fundamental piece of the Koebe net, the closeness of $\partial_{(v,b)}k_{\boxplus}$ can be expressed as

$$(43) \quad \frac{1}{\sqrt{q}} \frac{\operatorname{dn} \beta_{v_s}}{\operatorname{sn} \beta_{v_s}} u_1 + \sqrt{q} \operatorname{cn} \beta_{v_c} u_2 + \frac{1}{\sqrt{q}} \operatorname{dn} \beta_{v_c} u_3 + \frac{1}{\sqrt{q}} \frac{\operatorname{cn} \beta_{v_s}}{\operatorname{sn} \beta_{v_s}} u_4 = 0$$

Reflecting the fundamental piece in the angle bisector between u_1 and u_4 at k_{v_s} defines a quadrilateral with edges parallel to the fundamental piece, satisfying

$$(44) \quad \frac{1}{\sqrt{q}} \frac{\operatorname{cn} \beta_{v_s}}{\operatorname{sn} \beta_{v_s}} u_1 + \frac{1}{\sqrt{q}} \operatorname{dn} \beta_{v_c} u_2 + \sqrt{q} \operatorname{cn} \beta_{v_c} u_3 + \frac{1}{\sqrt{q}} \frac{\operatorname{dn} \beta_{v_s}}{\operatorname{sn} \beta_{v_s}} u_4 = 0.$$

The half sum and difference of the identities (43) and (44) yield two additional closed quadrilaterals with parallel edges. In particular, with (40) it is

$$\begin{aligned} \frac{1}{2} ((43) + (44)) &= d_{v_s} u_1 + d_{v_c} u_2 + d_{v_c} u_3 + d_{v_s} u_4 = 0, \\ \frac{1}{2} ((43) - (44)) &= d_{v_s}^* u_1 - d_{v_c}^* u_2 + d_{v_c}^* u_3 - d_{v_s}^* u_4 = 0. \end{aligned}$$

This proves that the one-forms (41) and (42) are closed, and their exactness follows. The minus signs in the second equation represent the change of orientation for vertical edges in the Christoffel dual. \square

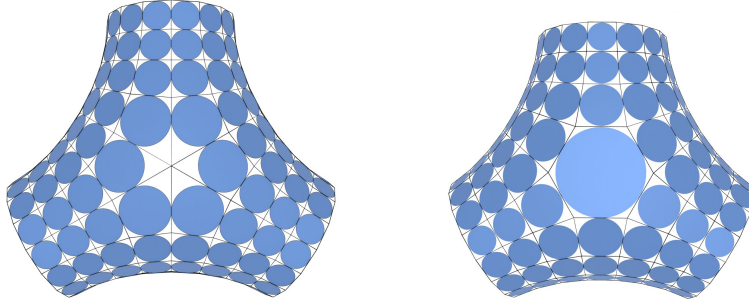


Figure 16. A pair of combinatorially dual S_1 -isothermic surfaces constructed using the method presented in Section 6. Corresponding dual edges are orthogonal. The umbilic point is represented by a vertex of even valence greater than four (left), or by a face of even valence greater than four (right).

By interchanging the roles of V_{\odot} and V_{\otimes} one obtains another, closely related, S_1 -cmc surface, see Figure 16. Circles of such S_1 -isothermic surfaces correspond to spheres of the other. The resulting surface pair is a principle binet in the sense of [5].

7. MINIMAL SURFACES IN THE LIMIT

Let s and s^* be an S_1 -cmc pair with Gauss map $n = c^* - c$ and constant mean curvature $H = 1$. Recall that a scaling of the surface pair, $s_\mu := \mu s, s_\mu^* := \mu s^*$, by a global factor μ changes the mean curvature to $H_\mu := \frac{1}{\mu}$ and the scaled center net c_μ^* becomes a normal offset surface of c_μ at distance $\frac{1}{H_\mu}$,

$$c_\mu^* = c_\mu + \frac{1}{H_\mu} n.$$

For $\mu \rightarrow \infty$ the mean curvature H_μ goes to zero, $H_\mu \rightarrow 0$, and the distance $\|c_\mu^* - c_\mu\| = \mu$ goes to infinity. Let us investigate this limit in more detail.

In the limit $q \rightarrow 1$ a ring pattern deforms to a circle pattern. Any rigid circle pattern can be deformed to a one-parameter ϵ -family of ring patterns, corresponding to $q = 1 - \epsilon$ with small ϵ with the same combinatorics and boundary data, see Section 5 and [11]. Let us consider the surfaces s_μ and s_μ^* with $\mu = \frac{1}{\epsilon}$ in the limit $\epsilon \rightarrow 0$. We will show that one of the surfaces converges to an S_1 -minimal surface while the dual surface converges to a Koebe net tangent to the unit sphere.

Theorem 7.1. *Consider a rigid spherical orthogonal circle pattern, i.e., with non-degenerate Hessian (33), and fixed boundary conditions, as well as its deformation to a spherical orthogonal ring pattern with $q = 1 - \epsilon$ and small ϵ . Then there exists an ϵ -family of associated S_1 -cmc pairs, $\frac{1}{\epsilon}s$ and $\frac{1}{\epsilon}s^*$ with mean curvature $H = \epsilon$. In the limit $\epsilon \rightarrow 0$, s converges to a classical Koebe net with the edges touching the unit sphere, and $\frac{1}{\epsilon}s^*$ converges to its dual S_1 -minimal surface.*

Proof. To analyze the behavior of the surfaces, we examine how the vertex sphere radii (40) evolve in the limit $\epsilon \rightarrow 0$. We want to emphasize that in the following the β -variables depend on the value of q but for simplicity we will write β_v instead of $\beta_v(q)$. For $q \rightarrow 1$ the Jacobi elliptic functions degenerate into hyperbolic trigonometric functions [44]:

$$(45) \quad \operatorname{sn}(z, q) \rightarrow \tanh(z), \quad \operatorname{cn}(z, q) \rightarrow \frac{1}{\cosh(z)}, \quad \operatorname{dn}(z, q) \rightarrow \frac{1}{\cosh(z)}.$$

PRIMAL RADII: For the scaled primal radii it is

$$\frac{1}{\epsilon} \lim_{q \rightarrow 1} \frac{1}{2\sqrt{q}} \left(\frac{\operatorname{dn}(\beta_v, q) + \operatorname{cn}(\beta_v, q)}{\operatorname{sn}(\beta_v, q)} \right) = \frac{1}{\epsilon} \frac{1}{\sinh(\beta_v)}.$$

We see that the primal radii go to infinity. However they remain finite for the normalized surface $s = \epsilon \frac{1}{\epsilon} s$.

DUAL RADII: To investigate the limit

$$(46) \quad \lim_{q \rightarrow 1} \frac{1}{1-q} \frac{1}{2\sqrt{q}} \left(\frac{\operatorname{dn}(\beta_v, q) - \operatorname{cn}(\beta_v, q)}{\operatorname{sn}(\beta_v, q)} \right) = \frac{1}{2 \tanh(\beta_v)} \lim_{q \rightarrow 1} \frac{\operatorname{dn}(\beta_v, q) - \operatorname{cn}(\beta_v, q)}{1-q}$$

we approximate cn and dn as follows

$$(47) \quad \begin{aligned} \operatorname{dn}(\beta_v, 1 - \epsilon) &= \frac{1}{\cosh(\beta_v)} + \epsilon a_{\operatorname{dn}} + o(\epsilon), \\ \operatorname{cn}(\beta_v, 1 - \epsilon) &= \frac{1}{\cosh(\beta_v)} + \epsilon a_{\operatorname{cn}} + o(\epsilon), \epsilon \rightarrow 0, \end{aligned}$$

with $a_{\text{cn}} := -\frac{\partial}{\partial q} \text{cn}(\beta_v, 1)$ and $a_{\text{dn}} := -\frac{\partial}{\partial q} \text{dn}(\beta_v, 1)$. Using the elementary identity $\text{cn}^2 + \text{sn}^2 = q^2 \text{sn}^2 + \text{dn}^2$ and thus

$$(\text{dn} - \text{cn})(\text{dn} + \text{cn}) = \epsilon(q + 1) \text{sn}^2$$

we find by comparing the sides in order ϵ :

$$a_{\text{dn}} - a_{\text{cn}} = \frac{\sinh^2(\beta_v)}{\cosh(\beta_v)}.$$

Substitution into (46) yields

$$\frac{1}{2 \tanh(\beta_v)} \lim_{q \rightarrow 1} \left(\frac{\text{dn}(\beta_v, q) - \text{cn}(\beta_v, q)}{1 - q} \right) = \frac{1}{2} \sinh(\beta_v).$$

During the limiting process the pair of surfaces may only be scaled simultaneously in order to keep the cmc properties of the pair. Afterwards the two surfaces can be treated separately. A global scaling of the primal surface in the limit allows to find a finite surface with vertex spheres of radii $\frac{1}{\sinh(\beta_v)}$. This scaling preserves the Christoffel duality.

In conclusion in the limit we obtain two S_1 -isothermic surfaces, s and $\frac{1}{\epsilon} s^*$, that are Christoffel dual with vertex sphere radii

$$d_v = \frac{1}{\sinh(\beta_v)} \quad \text{and} \quad d_v^* = \frac{1}{2} \sinh(\beta_v).$$

In the limit $q \rightarrow 1$ the spheres S_{\pm}^2 of the two-sphere Koebe net n converge to the unit sphere, and n becomes a classical Koebe net with all edges touching the unit sphere. Further,

$$s = n + s^* \xrightarrow{\epsilon \rightarrow 0} n$$

since $\frac{1}{\epsilon} s^*$ stays finite. Thus the surfaces s and $\frac{1}{\epsilon} s^*$ indeed form a Koebe net and an S_1 -minimal surface, and in the limit $\epsilon \rightarrow 0$ we recovered the description of S_1 -minimal surfaces from [15]. \square

8. EXAMPLES OF CMC SURFACES IN \mathbb{R}^3

We apply the method described in Section 6 to construct concrete examples of S-cmc surfaces in \mathbb{R}^3 . We restrict the underlying S-quad graphs to combinatorial rectangles. Under suitable boundary conditions these combinatorial rectangles will lead to fundamental pieces of reflectionally symmetric cmc surfaces. Umbilic points, or vertices with valence greater than four, can appear at the corners of these fundamental pieces after reflection.

Let us consider the case when a fundamental piece of a reflectionally symmetric smooth cmc surface is bounded by four curvature lines, each lying in a (reflection) plane, see [13]. The Gauss map along these curvature lines forms a spherical quadrilateral whose edges are segments of great circles. At corners that are not exceptional, the curvature lines and their Gauss image intersect at an angle $\frac{\pi}{2}$. At exceptional vertices, the curvature lines of the surface intersect at an angle $\frac{\pi}{n}$, their Gauss images at an angle $\pi - \frac{\pi}{n}$. These boundary angles and a sampling of curvature lines provide initial data for constructing a fundamental piece of an orthogonal ring pattern using the variational principle.

We choose the parameter q so that the orthogonal ring pattern is bounded by the same spherical quadrilateral as the smooth Gauss map, ensuring that the ring pattern

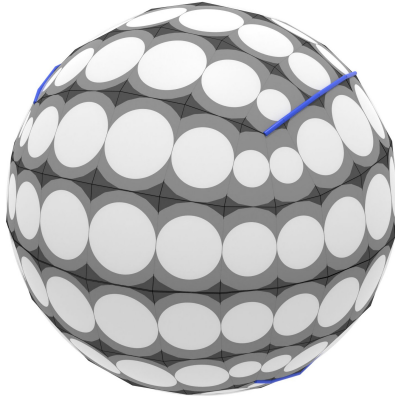


Figure 17. A two-sphere Koebe net forming a double cover of the sphere, one layer of the covering is shown. In the figure exceptional vertices are adjacent to three copies of a fundamental piece. The cuts of the covering, shown in blue, connect two exceptional vertices.

retains the same reflection symmetries. In this case we can construct closed examples of (reflectionally symmetric) two-sphere Koebe nets, see Figure 17. Self intersections and double covers occur.

After constructing the fundamental piece, the corresponding reflections determine the complete discrete periodic cmc surface.

8.1. Doubly periodic S_1 -cmc surfaces. Cmc surfaces in Euclidean three-dimensional space are isometric to minimal surfaces in the three-dimensional sphere S^3 . This fact is known as the classical Lawson correspondence [41]. Lawson first used this approach to show the existence of two reflectionally symmetric, doubly periodic cmc surfaces in \mathbb{R}^3 , denoted by $\psi(U_{2,2})$ and $\psi(U_{3,3})$, where ψ denotes the immersion of the conjugate surfaces into \mathbb{R}^3 . The isometric minimal surfaces in S^3 are the classical Lawson surfaces $\xi_{2,2}$ and $\xi_{3,3}$, while $U_{2,2}$ and $U_{3,3}$ denote their universal Riemannian coverings. The integers refer to the symmetry group of the surface, and the fundamental pieces of $U_{2,2}$ and $U_{3,3}$ are obtained by solving the corresponding Plateau problem in S^3 .

The smooth cmc surfaces $\psi(U_{2,2})$ and $\psi(U_{3,3})$ have recently been constructed in [13] using the DPW method [24]. They are shown, together with their discrete analogues and corresponding orthogonal ring patterns, in Figure 18. In these doubly periodic examples, the spherical quadrilateral bounding the fundamental piece of the Gauss map degenerates into a triangle.

We want to emphasize that the smooth surfaces on the left in Figure 18 and their discrete counterparts on the right are constructed using entirely different methods.

8.2. Triply periodic S_1 -cmc surfaces. In the 1880s, Schwarz discovered several triply periodic minimal surfaces [50], which were later extended by Schoen [47]. Two examples are the Schwarz P surface and Schoen's I-WP surface. The surfaces admit reflective symmetries and allow deformations into triply periodic surfaces of constant mean curvature [37], which retain the same reflective symmetries as their minimal counterparts. The existence of the cmc deformations is proven by solving Plateau problems in S^3 . The

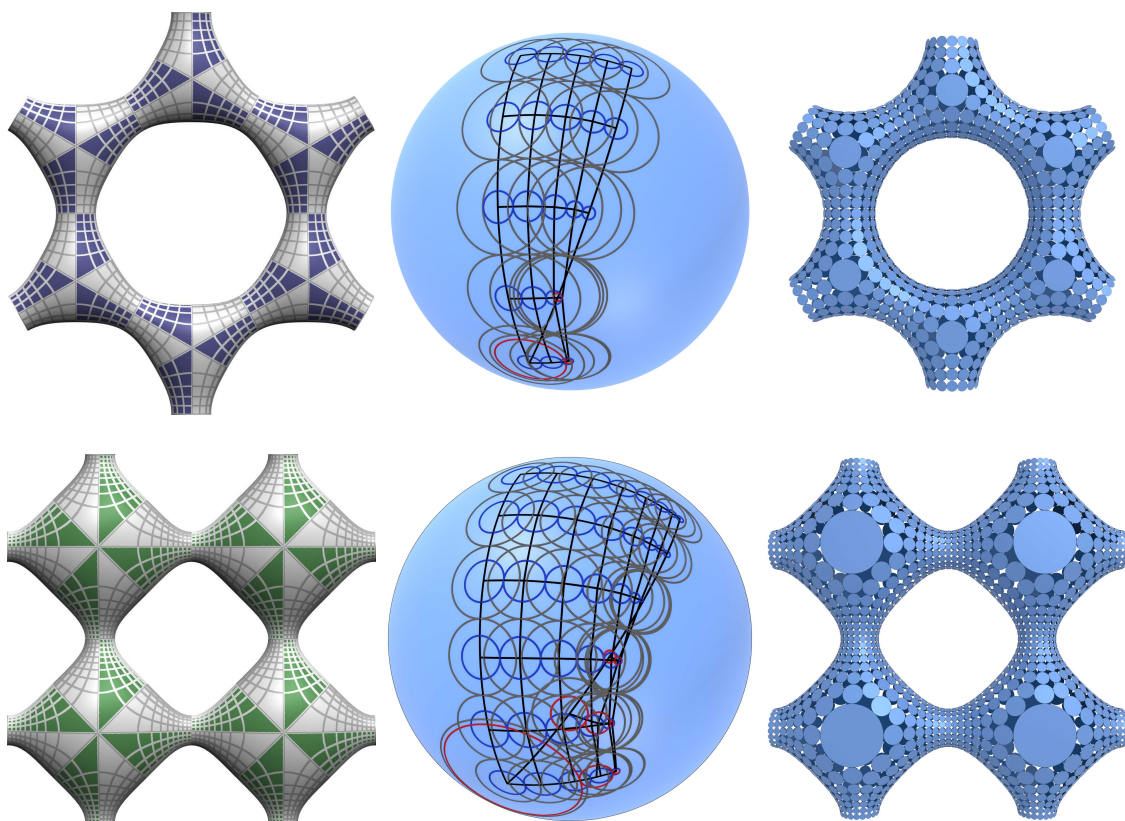


Figure 18. The doubly periodic cmc surfaces $\psi(U_{2,2})$ (top) and $\psi(U_{3,3})$ (bottom) with hexagonal and quadrilateral lattice symmetry, respectively. The rows show the smooth cmc surfaces, the orthogonal ring patterns (only half of the rings are shown), and the discrete cmc surfaces. The shape of the orthogonal ring patterns is determined by the nominal angles at the corners, $\frac{\pi}{2}, \frac{2\pi}{3}, \frac{\pi}{2}, \frac{\pi}{2}$ and $\frac{\pi}{2}, \frac{\pi}{4}, \frac{\pi}{2}, \frac{\pi}{2}$, and the global parameter, $q \approx 0.982889$ and $q \approx 0.991636$, respectively.

Lawson correspondence is used to generate the corresponding cmc surfaces in \mathbb{R}^3 [37]. Discrete Schwarz P surfaces with mean curvature $H < 0$, $H = 0$ and $H > 0$ are shown in Figure 19.

In [13] a smooth Schwarz P cmc surface and Schoen's I-WP cmc surface have been constructed using the DPW method [24]. They are shown, together with their discretizations and orthogonal ring patterns, in Figure 1. The shape of the orthogonal ring pattern for the Schwarz P surface is determined by the nominal angles $\frac{\pi}{2}, \frac{2\pi}{3}, \frac{\pi}{2}, \frac{\pi}{2}$ at the corners and the parameter $q \approx 0.995798$. Similarly, the orthogonal ring pattern for Schoen's I-WP surface has cone angles $\frac{\pi}{2}, \frac{2\pi}{3}, \frac{3\pi}{4}, \frac{\pi}{2}$ at the corners and parameter $q \approx 0.994351$. Note that the fundamental piece of the Schwarz P surface has the same boundary cone angles as the doubly periodic surface $\psi(U_{2,2})$ of Section 8.1, only the global parameter q is different.

Our numerical experiments with discrete cmc surfaces show an astonishingly good convergence. It would be desirable to give a mathematical proof of this fact. For discrete minimal surfaces the convergence is proven to be C^∞ [40].

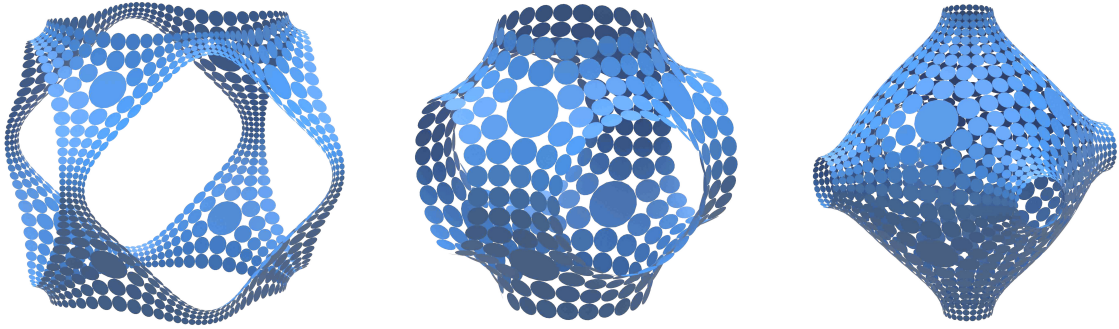


Figure 19. S_1 -isothermic discrete Schwarz P minimal surface (center) and Schwarz P cmc surfaces, with negative mean curvature (left) and positive mean curvature (right). The fundamental pieces of the underlying S-quad graph correspond to combinatorial rectangles with dimensions (n, m) , (m, m) and (m, n) , respectively, where $n > m$. The Gauss map for all three surfaces is bounded by the same spherical quadrilateral, indicating that the surfaces share the same reflectional symmetries.

9. DISCRETE S-ISOTHERMIC SURFACES IN $\mathbb{R}^{2,1}$

In the remaining sections of this paper, we will translate the geometric constructions from the first part from \mathbb{R}^3 to the Lorentz space $\mathbb{R}^{2,1}$, with the goal of constructing discrete spacelike cmc surfaces in $\mathbb{R}^{2,1}$. We will show that, with a method analogous to the construction scheme of discrete cmc surfaces in \mathbb{R}^3 , one can construct discrete spacelike cmc surfaces in $\mathbb{R}^{2,1}$, see e.g. [43, 36] for a differential geometric treatment of (spacelike cmc) surfaces in $\mathbb{R}^{2,1}$. Furthermore, we will show that the discrete Gauss map of the discrete spacelike cmc surfaces corresponds to spacelike two-sphere Koebe nets and hyperbolic orthogonal ring patterns [11].

To define spacelike S-isothermic nets in $\mathbb{R}^{2,1}$, we first introduce some basic geometric facts and Möbius geometry of $\mathbb{R}^{2,1}$. Note that in literature the conformal compactification of $\mathbb{R}^{2,1}$ is also denoted as the Einstein universe [6] and the geometry as pseudo-conformal geometry. We stick to the naming conventions *Möbius quadric* and *Möbius geometry* as our treatment is close to the Euclidean case.

The Lorentz space $\mathbb{R}^{2,1}$ is equipped with the non-degenerate bilinear form

$$(48) \quad \langle x, y \rangle = x_1y_1 + x_2y_2 - x_3y_3$$

of signature $(++-)$. Lines and planes in $\mathbb{R}^{2,1}$ are called *spacelike*, *isotropic* or *timelike* depending on the signature of the induced metric on the subspaces. For example, planes can have signatures $(++)$, $(+0)$ or $(+-)$ and corresponding normal vectors of signature $(-)$, (0) or $(+)$, respectively. The three types of planes and the *light cone*, consisting of all isotropic lines, are shown in Figure 20 (left).

A spacelike surface surface in $\mathbb{R}^{2,1}$ is a surface such that the induced metric of the surface is positive definite (i.e. a Riemannian metric). Its unit normal field consists of timelike vectors, the normal vectors are orthogonal to the spacelike tangent planes.

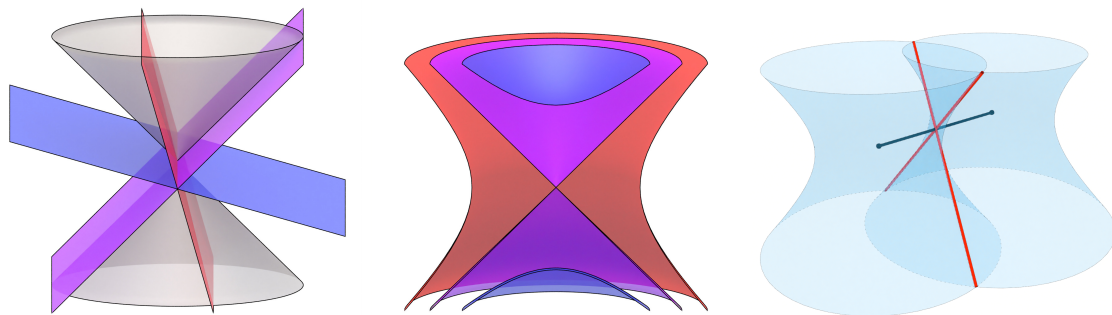


Figure 20. Left: A spacelike plane (blue), an isotropic plane (violet), a timelike plane (red), and the light cone (gray) in $\mathbb{R}^{2,1}$. Center: A spacelike sphere (blue), a null sphere (violet), and a timelike sphere (red). Right: Two touching timelike spheres.

A sphere in Lorentzian space with center c and squared radius d^2 is given by the point set

$$s_{c,d^2} := \{x \in \mathbb{R}^{2,1} \mid \langle x - c, x - c \rangle = d^2\}.$$

The squared radius d^2 can be positive, zero, or negative. The three types of spheres are called *spacelike*, *null* and *timelike* spheres and correspond to the cases $d^2 < 0$, $d^2 = 0$ and $d^2 > 0$, respectively. From an Euclidean point of view they correspond to two-sheeted hyperboloids, two-dimensional cones and one-sheeted hyperboloids, see Figure 20 (center).

Two timelike spheres *touch* if they share a common point t and have the same tangent plane at that point. This touching condition implies that the two spheres share two generators that intersect at t , see Figure 20 (right). The line connecting the centers of the spheres is spacelike, passes through t , and is orthogonal to the common timelike tangent plane.

Non-empty planar sections of spheres are *spacelike*, *null* or *timelike Lorentz circles*. Our primary examples we will be spacelike circles contained in spacelike planes, which correspond to ellipses from a Euclidean point of view. In addition, we will encounter spacelike circles contained in timelike planes which correspond to hyperbolas with a timelike axis. Note that timelike planes can contain not only spacelike circles, but also null circles (such as the one-dimensional cones in the common tangent plane of two touching timelike spheres) and timelike circles (which correspond to hyperbolas with a spacelike axis).

To study Möbius geometry of $\mathbb{R}^{2,1}$ we are using $\mathbb{R}^{3,2}$, which is equipped with the non-degenerate bilinear form

$$(49) \quad \langle x, y \rangle_{3,2} = x_1y_1 + x_2y_2 + x_3y_3 - x_4y_4 - x_5y_5.$$

For the standard basis e_1, \dots, e_5 of $\mathbb{R}^{3,2}$ we introduce new basis vectors $e_0 := \frac{1}{2}(e_5 - e_3)$ and $e_\infty := \frac{1}{2}(e_3 + e_5)$. Let

$$\hat{\mathbb{S}}_0 := \{\hat{x} \in \mathbb{R}^{3,2} \mid \langle \hat{x}, \hat{x} \rangle_{3,2} = 0\}$$

be the light cone in $\mathbb{R}^{3,2}$. Points of $\mathbb{R}^{2,1} \cup \{\infty\}$ can be identified with points of $\hat{\mathbb{S}}_0$ via the identification

$$(50) \quad \mathbb{R}^{2,1} \ni x \leftrightarrow \hat{x} = x + e_0 + \|x\|^2 e_\infty \in \hat{\mathbb{S}}_0.$$

In this context, x on the right hand side is understood as $x_1 e_1 + x_2 e_2 + x_3 e_4 \in \mathbb{R}^{3,2}$, and points of the form $\hat{x} = x + e_0 + \|x\|^2 e_\infty \in \hat{\mathbb{S}}_0$ are normalized so that $\langle \hat{x}, e_\infty \rangle_{4,1} = -\frac{1}{2}$. The point $\infty \in \mathbb{R}^3 \cup \{\infty\}$ is identified with e_∞ . If we interpret $\mathbb{R}^{3,2}$ as the space of homogeneous coordinates of \mathbb{RP}^4 , points on

$$\mathcal{M} := \{[\hat{x}] \in \mathbb{RP}^4 \mid \langle \hat{x}, \hat{x} \rangle_{3,2} = 0\},$$

which is called the *Möbius quadric* of $\mathbb{R}^{2,1}$, can be identified with null spheres in $\mathbb{R}^{2,1}$. A point of the form (50) in $\hat{\mathbb{S}}_0$ represents a special choice of homogeneous coordinates for the corresponding projective point in \mathcal{M} , and it represents the center of the null sphere. Points inside the Möbius quadric,

$$[\hat{x}] \in \mathcal{M}_- := \{[\hat{x}] \in \mathbb{RP}^4 \mid \langle \hat{x}, \hat{x} \rangle_{3,2} < 0\},$$

can be identified with non-oriented spacelike spheres in $\mathbb{R}^{2,1}$, points outside the Möbius quadric,

$$[\hat{x}] \in \mathcal{M}_+ := \{[\hat{x}] \in \mathbb{RP}^4 \mid \langle \hat{x}, \hat{x} \rangle_{3,2} > 0\},$$

can be identified with non-oriented timelike spheres in \mathbb{R}^3 . Hyperplanes are considered as (spacelike, isotropic, timelike) spheres with infinite radius.

We will further consider Möbius geometry of timelike spheres in more detail. A timelike sphere with center c and radius d^2 is represented by the projective point

$$(51) \quad [\hat{s}] = [c + e_0 + (\|c\|^2 - d^2)e_\infty] \in \mathcal{M}_+.$$

Its homogeneous coordinates can be normalized to

$$(52) \quad \hat{s} = \frac{1}{d} (c + e_0 + (\|c\|^2 - d^2)e_\infty),$$

which is a point on the Lorentz unit sphere

$$\hat{\mathbb{S}}_1 := \{\hat{x} \in \mathbb{R}^{3,2} \mid \langle \hat{x}, \hat{x} \rangle_{3,2} = 1\} \subset \mathbb{R}^{3,2}.$$

Recall that for the squared radius of timelike spheres $d^2 > 0$, so its square root d is always real. One can associate a sign to d that encodes the orientation of the sphere. The two points (52) with $\pm d$ correspond to the same point (51) in \mathcal{M}_+ .

To study spacelike S-isothermic surfaces, let us recall the combinatorics of \mathcal{G} , a quad graph with interior vertices of even valence and edges divided into 'horizontal' and 'vertical' edges, as shown in Figure 2.

Definition 9.1. *A map*

$$s : V(\mathcal{G}) \rightarrow \{\text{oriented timelike spheres in } \mathbb{R}^{2,1}\}$$

is called a discrete spacelike S-isothermic surface if the following conditions hold:

- (i) *The centers of four oriented spheres associated with a face of \mathcal{G} lie on a spacelike plane.*

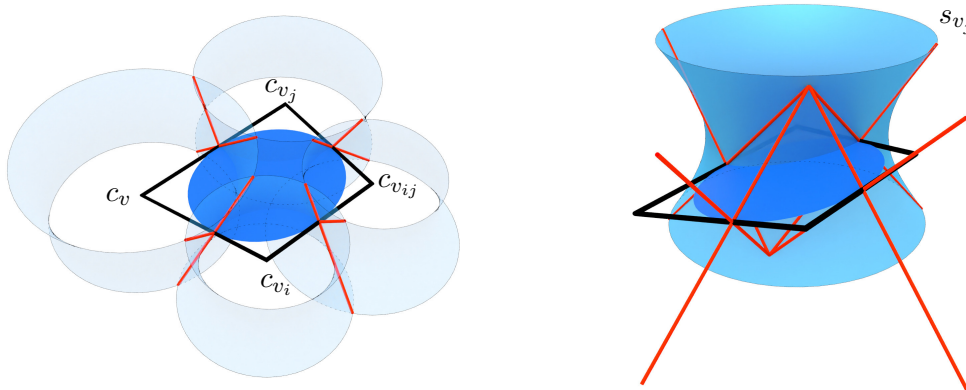


Figure 21. A spacelike S_1 -isothermic quadrilateral. Neighboring spheres touch and have a common orthogonal circle (left). The four spheres intersect in two points that form the centers of two null spheres that contain the orthogonal circle (right).

(ii) The corresponding map $\hat{s} : V(\mathcal{G}) \rightarrow \hat{\mathbb{S}}_1 \subset \mathbb{R}^{3,2}$, that maps oriented timelike spheres to

$$\hat{s} = \frac{1}{d} (c + e_0 + (\|c\|^2 - d^2)e_\infty),$$

satisfies the discrete Moutard equation

$$(53) \quad \hat{s}_{v_{ij}} - \hat{s}_v = a_{ij}(\hat{s}_{v_j} - \hat{s}_{v_i})$$

for some $a_{ij} : F(\mathcal{G}) \rightarrow \mathbb{R}$.

The vertex spheres of a spacelike discrete S-isothermic surface are timelike. Their positive squared radius corresponds to the positive metric of the surface. The labeling property (cf. (4)) also holds for spacelike S-isothermic surfaces

$$\begin{aligned} \langle \hat{s}_v, \hat{s}_{v_i} \rangle_{3,2} &= \langle \hat{s}_{v_j}, \hat{s}_{v_{ij}} \rangle_{3,2} =: \alpha_i \\ \langle \hat{s}_v, \hat{s}_{v_j} \rangle_{3,2} &= \langle \hat{s}_{v_i}, \hat{s}_{v_{ij}} \rangle_{3,2} =: \alpha_j. \end{aligned}$$

The elementary quadrilaterals of a spacelike S-isothermic surface are called *spacelike S-isothermic quadrilaterals*. There are three types of spacelike S-isothermic quadrilaterals, analogous to the three types in \mathbb{R}^3 presented in Figure 3, but with different geometric properties. A special case are those with touching vertex spheres, called *spacelike S_1 -isothermic quadrilaterals*.

Proposition 9.2. *Spacelike S_1 -isothermic quadrilaterals have spacelike incircles that intersect the four adjacent spheres orthogonally. The four timelike vertex spheres intersect at two points which are the centers of the two null spheres containing the orthogonal circle, see Figure 21.*

Proof. The faces of the net \hat{s} in $\mathbb{R}^{3,2}$ are planar. Similar to the proof of Corollary 2.2, we consider the linear subspace containing a face of \hat{s} . The orthogonal complement of the linear subspace is of signature (1, 1). Thus it represents (in contrast to the Euclidean case) a circle that intersects the four spheres associated to the face orthogonally and that is, by definition, spacelike. Furthermore, the orthogonal complement having signature (1, 1)

also implies that the four spheres in $\mathbb{R}^{2,1}$ are orthogonal to two null spheres and thus in particular intersect in their centers. For more details we refer to [3]. \square

The *Christoffel dual* s^* of a spacelike S_1 -isothermic surface s can be defined analogously to the \mathbb{R}^3 case by the exact one-form ∂c^* defined by

$$\partial_{(v,v')}c^* = \frac{\partial_{(v,v')}c}{d_v d_{v'}}.$$

Recall that

$$c : V(\mathcal{G}) \rightarrow \mathbb{R}^{2,1}, \quad v \mapsto c_v$$

denotes the center net of s and $d : V(\mathcal{G}) \rightarrow \mathbb{R}$, $v \mapsto d_v$ the corresponding signed radii. For spacelike S_1 -isothermic surfaces s and s^* let c_f, c_f^* and d_f, d_f^* denote the centers and radii of the spacelike orthogonal face circles.

A spacelike S_1 -isothermic surface and its Christoffel dual have the following properties:

- (i) The Christoffel dual of a spacelike S_1 -isothermic net is a spacelike S_1 -isothermic net.
- (ii) The radii of the vertex spheres are related by $d_v^* = \frac{1}{d_v}$.
- (iii) Orthogonal circle radii are related by $d_f^* = \frac{1}{d_f}$.

In general, the Christoffel dual is defined up to global scaling, thus

$$(54) \quad d_v d_v^* = d_f d_f^* = \lambda$$

for a $\lambda \in \mathbb{R}$.

10. DISCRETE CMC SURFACES IN $\mathbb{R}^{2,1}$

Definition 10.1. *Two S -isothermic surfaces s and s^+ are called a timelike Darboux pair if the corresponding Moutard nets $\hat{s}, \hat{s}^+ : V(\mathcal{G}) \rightarrow \mathbb{R}^{3,2}$ are related by a Moutard transformation,*

$$\hat{s}_{v'}^+ - \hat{s}_v = a_+(\hat{s}_v^+ - \hat{s}_{v'})$$

with some $a_+ : E(\mathcal{G}) \rightarrow \mathbb{R}$, and the normal vectors connecting corresponding vertex sphere centers,

$$(55) \quad n_v := c_v^* - c_v,$$

are timelike. In this case, one surface is called a timelike Darboux transform of the other.

The normal vectors of smooth spacelike surfaces in $\mathbb{R}^{2,1}$ are timelike. The vectors (55) will serve as the discrete Gauss map for the following definition of S-cmc surfaces and are therefore restricted to be timelike. Timelike Darboux transforms preserve the edge labels α_i and α_j given in (53). Associated with a timelike Darboux transform is a constant parameter α given by

$$(56) \quad -2\alpha := -2\langle \hat{s}_v, \hat{s}_v^+ \rangle_{3,2} = \|c_v - c_v^+\|^2 - (d_v^2 + d_v^{+2}).$$

Definition 10.2. *A spacelike S -isothermic surface s is a spacelike S-cmc surface, if its Christoffel dual simultaneously is a timelike Darboux transform (after appropriate scaling and translation).*

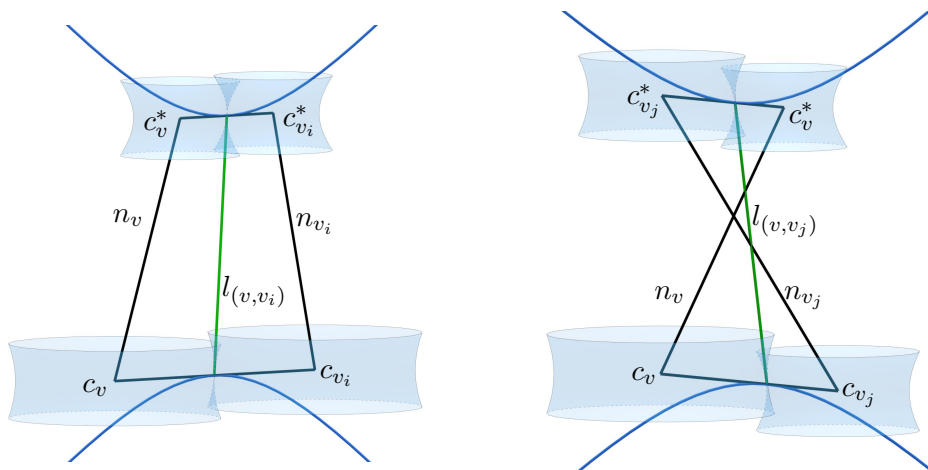


Figure 22. The two types of transformation faces of a spacelike S_1 -cmc pair together with vertex normals (black) and edge normals (green). The circle orthogonal to the four adjacent vertex spheres (blue) is spacelike. Embedded faces correspond to horizontal edges, non-embedded faces correspond to vertical edges.

We now restrict ourselves to the case of touching spheres, i.e., spacelike S_1 -cmc surfaces. A fundamental hexahedron of a Lorentz S_1 -cmc surface pair has the same properties as in the Euclidean case, see Figure 7, also for notation. In particular, the normal vectors have the following properties. The *vertex normals*

$$(57) \quad n : V(\mathcal{G}) \rightarrow \mathbb{R}^{2,1}, \quad v \mapsto n_v := c_v^* - c_v,$$

connect centers of primal and dual spheres. They are timelike per definition.

The *edge normals*

$$(58) \quad l : E(\mathcal{G}) \rightarrow \mathbb{R}^{2,1}, \quad (v, v') \mapsto l_{(v,v')} := t_{(v,v')}^* - t_{(v,v')}$$

connect touching points of vertex spheres. They are orthogonal to the parallel pair of primal and dual edge and they lie in timelike planes containing the pair of parallel edges, and are therefore timelike. They are of squared lengths

$$(59) \quad \Delta_i^2 := -2\alpha + 2\lambda \quad \text{or} \quad \Delta_j^2 := -2\alpha - 2\lambda,$$

depending on the label of the corresponding pair of parallel edges, see Figure 22. Here α denotes the parameter of the Darboux transform (56) and λ denotes the global constant (54). Note that $\Delta_j^2 < \Delta_i^2 < 0$.

The *face normals*

$$(60) \quad m : F(\mathcal{G}) \rightarrow \mathbb{R}^{2,1}, \quad f \mapsto m_f := c_f^* - c_f$$

connect centers of primal and dual orthogonal circles. The circles are coaxial and the face normals are orthogonal to the parallel spacelike faces.

Definition 10.3. A Q -net $k : V(\mathcal{G}) \rightarrow \mathbb{R}^{2,1}$ is called a spacelike two-sphere Koebe net if its edges alternately touch two spacelike spheres S_+^2 and S_-^2 (concentric with the spacelike unit sphere) whose squared radii satisfy the relation $r_+^2 r_-^2 = 1$.

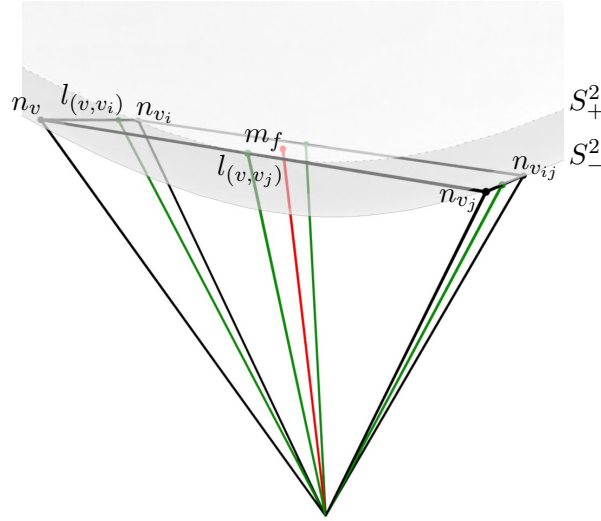


Figure 23. The Gauss image of a fundamental spacelike S_1 -cmc hexahedron, which forms a face of a spacelike two-sphere Koebe net, alternately tangent to the two spacelike spheres S_+^2 and S_-^2 . The points of tangency are given by the edge normal vectors $l_{(v,v')} \in S_\pm^2$ (green). Horizontal edges always touch S_-^2 and vertical edges always touch S_+^2 . The vector m_f (red) is orthogonal to the planar face.

Recall that in Section 3.2 we introduced the discrete mean curvature H for pairs of discrete surfaces with parallel edges in \mathbb{R}^3 . Since we restrict our considerations to discrete spacelike surfaces, that is discrete surfaces with positive metric, the considerations for \mathbb{R}^3 can be applied directly and analogously to the case of spacelike discrete surfaces with parallel edges in $\mathbb{R}^{2,1}$.

The following theorem can be proved analogously to Theorems 3.6 and 3.9.

Theorem 10.4. *Let s and s^* be a (suitably scaled) spacelike S_1 -cmc pair. The Gauss map*

$$(61) \quad n : V(\mathcal{G}) \rightarrow \mathbb{R}^{2,1}, \quad v \mapsto n_v := c_v^* - c_v,$$

between the sphere centers of s and s^ , forms a spacelike two-sphere Koebe net. Furthermore, the pair (s, n) of an S_1 -cmc surface and its Gauss map has constant discrete mean curvature $H = 1$.*

11. SPACELIKE TWO-SPHERE KOEBE NETS AND HYPERBOLIC ORTHOGONAL RING PATTERNS

In this section, we will study the correspondence between pairs of spacelike dual two-sphere Koebe nets and hyperbolic orthogonal ring patterns. Properties derived analogously to those in the correspondence between two-sphere Koebe nets in \mathbb{R}^3 and spherical orthogonal ring patterns remain without a proof. For a more detailed consideration we refer to Section 4.

Let k^s and k^c be a pair of regular, dual spacelike two-sphere Koebe nets (cf. Definition 4.2) with underlying S-quad graph \mathcal{S} (cf. Definition 4.1), which alternately touch the upper

parts of two spacelike spheres S_+^2 and S_-^2 . The spheres S_+^2 and S_-^2 with radii r_+^2 and r_-^2 are assumed to be concentric with the spacelike unit sphere $S^2 := \{x \in \mathbb{R}^{2,1} \mid \langle x, x \rangle = -1\} \subset \mathbb{R}^{2,1}$. The upper parts of S_+^2 and S_-^2 are given by

$$S_\pm^2 := \{x \in \mathbb{R}^{2,1} \mid \langle x, x \rangle = r_\pm^2, x_3 > 0\}.$$

The squared radii r_+^2 and r_-^2 are negative, by $|r_+|$ and $|r_-|$ we denote the absolute values of their imaginary square roots. Analogously, we introduce the notation

$$(62) \quad |x| := |\sqrt{\langle x, x \rangle}| \quad \text{for } x \in \mathbb{R}^{2,1}.$$

Projecting timelike vectors onto S^2 corresponds to normalizing the vectors with (62). In particular, for vertices k_v and tangent points t_b^\pm of either k^s or k^c , let

$$p_v := \frac{k_v}{|k_v|}, \quad q_b := \frac{t_b^+}{|r^+|} = \frac{t_b^-}{|r^-|}$$

denote their projection onto S^2 . The upper part of S^2 can be interpreted as the hyperboloid model of the hyperbolic plane H^2 embedded in $\mathbb{R}^{2,1}$. One can associate hyperbolic rings (pairs of concentric hyperbolic circles) with the white vertices $v \in V_w(\mathcal{S})$, centered at p_v with hyperbolic radii (determined up to sign)

$$\cosh(r_v) = \frac{|r_-|}{|k_v|}, \quad \cosh(R_v) = \frac{|r_+|}{|k_v|}.$$

Here r_v always denotes the smaller radius (of the inner circle) and R_v the larger radius (of the outer circle) of the ring. Each ring passes through the projection of adjacent tangent points q_b . Two rings corresponding to white vertices of a face of \mathcal{S} , see Figure 9 (right), intersect orthogonally, i.e., the inner circle of one ring intersects the outer circle of the other ring orthogonally, and vice versa. The rings form a hyperbolic orthogonal ring pattern [11], see Figure 24.

For hyperbolic orthogonal ring patterns there exists a global constant $q < 1$ such that the radii of inner and outer circles of all rings are related by

$$(63) \quad q \cosh R_v = \cosh r_v.$$

This follows from the orthogonality of the rings and the hyperbolic Pythagorean theorem. Conversely, lift the centers p_v of the hyperbolic rings to

$$(64) \quad k_v := \frac{\sqrt{q}}{\cosh(r_v)} p_v = \frac{1}{\sqrt{q} \cosh(R_v)} p_v,$$

and the touching points q_b to the two points

$$(65) \quad t_b^+ := \frac{1}{\sqrt{q}} q_b, \quad t_b^- := \sqrt{q} q_b.$$

Restricting \mathcal{S} to the two graphs \mathcal{G} and \mathcal{G}^* , see Figure 9 (left), we obtain two combinatorially dual, polyhedral surfaces with vertices (64). They form a pair of dual spacelike two-sphere Koebe nets. They are alternately tangent to the upper part of the spacelike spheres S_+^2 and S_-^2 where the points of tangency are given by (65). The spacelike spheres S_+^2 and S_-^2 are of squared radii $-\frac{1}{q}$ and $-q$, respectively. We obtain a correspondence analogous to the one between dual two-sphere Koebe nets and spherical orthogonal ring pattern (cf. Theorem 4.6).

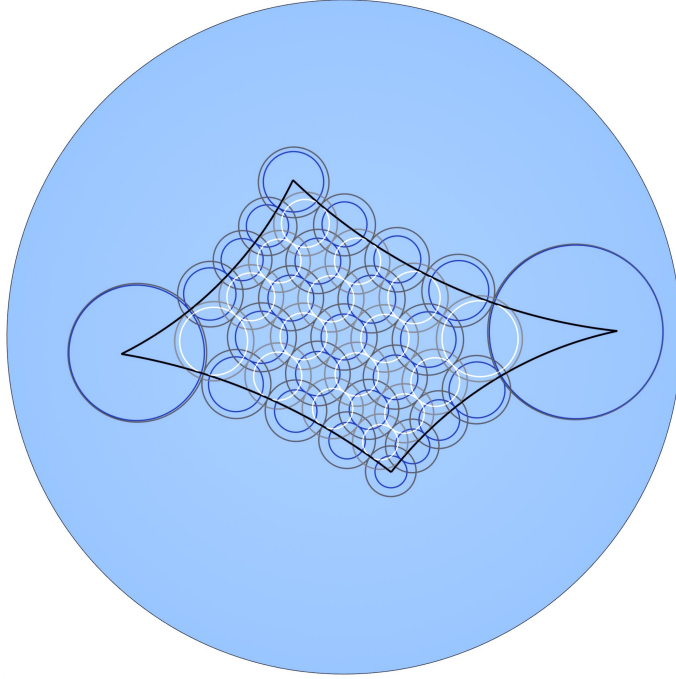


Figure 24. A hyperbolic orthogonal ring pattern, shown in the Poincaré disk model, with $q = 0.99$ and angles π for the boundary vertices and $\frac{\pi}{2}, \frac{\pi}{10}, \frac{2\pi}{5}, \frac{\pi}{5}$ for the four corner vertices.

Theorem 11.1. *Pairs of regular, dual spacelike two-sphere Koebe nets touching the upper parts of the spacelike spheres S_+^2 and S_-^2 , with radii of absolute values $|r_+|$ and $|r_-|$, are in one to one correspondence to hyperbolic orthogonal ring patterns in the hyperbolic plane with global parameter $q = \frac{|r_-|}{|r_+|}$. Vertices of the Koebe nets correspond to centers of hyperbolic rings, while points of tangency of the Koebe nets correspond to touching points of the rings.*

Hyperbolic orthogonal ring patterns allow a variational description that can be derived in a way analogous to the spherical case. We give a brief overview here and refer to Section 4 and to [11] for further details proofs.

Recall that by \mathcal{S}_z we denote an S-quad graph defined by a simply connected subset of squares of the \mathbb{Z}^2 lattice in \mathbb{R}^2 , and by V_B the set of its white boundary vertices. Our main example is the combinatorial rectangle (27).

Due to (63) one can uniformize the hyperbolic ring radii R_v and r_v in terms of Jacobi elliptic functions:

$$(66) \quad \cosh R_v = \frac{1}{q \operatorname{sn}(\gamma_v, q)}, \quad \tanh R_v = \operatorname{dn}(\gamma_v, q), \quad \sinh r_v = \frac{\operatorname{cn}(\gamma_v, q)}{\operatorname{sn}(\gamma_v, q)},$$

where $\gamma_v \in [0, 2K]$ for $(r_v, R_v) \in [-\infty, \infty] \times [R_0, \infty]$, and $\cosh R_0 = 1/q$. Using the function F from (30) one defines the functional

$$(67) \quad S_{hyp}(\gamma) := \sum_{(v,v')} (F(\gamma_v - \gamma_{v'}) + F(\gamma_v + \gamma_{v'})) + \sum_v \Phi_v \gamma_v,$$

where the first sum is taken over all pairs of white vertices corresponding to neighboring rings and the second sum is taken over all white vertices $v \in V_w(\mathcal{S}_z)$. Critical points γ of this functional with appropriately chosen Φ_v correspond to the radii of the rings of hyperbolic orthogonal ring patterns. Remarkably, the functional (67) is convex. Its minimization allows to construct hyperbolic orthogonal ring patterns from suitable boundary data, and one can prove their existence and uniqueness [11].

Theorem 11.2. *Let \mathcal{S}_z be a combinatorial rectangle (27) with white corner vertices and white boundary vertices V_B . Further let $q \leq 1$. Hyperbolic orthogonal ring patterns can be obtained as solutions of the following boundary value problems:*

- *(Dirichlet boundary conditions) For any choice of prescribed radii $\gamma : V_B \rightarrow [0, 2K]$ of boundary rings there exists a unique hyperbolic orthogonal ring pattern with these boundary radii.*
- *(Neumann boundary conditions) Let $\Theta : V_B \rightarrow (-2\pi, 2\pi)$ be prescribed boundary cone angles such that $|\Theta_v| < \pi$ at the corners. Then there exists a unique hyperbolic orthogonal ring pattern \mathcal{R} with these boundary cone angles.*

Moreover, the solution of the Neumann boundary value problem is given by the unique minimizer of the functional (67) with $\Phi_v = -2\pi$ for all inner vertices, $\Phi_v = -\Theta_v$ for all positively oriented boundary rings, $\Phi_v = -\Theta_v - \pi$ for negatively oriented corners, and $\Phi_v = -\Theta_v - 2\pi$ for other negatively oriented boundary rings.

For $q = 1$ one obtains a hyperbolic orthogonal circle pattern. The circle radii in terms of the γ -variables, which we denote by γ^0 , are given by

$$\cosh R = \coth \gamma^0, \quad \sinh R = \frac{1}{\sinh \gamma^0}.$$

12. CONSTRUCTING CMC SURFACES IN $\mathbb{R}^{2,1}$

The construction scheme for cmc surfaces in $\mathbb{R}^{2,1}$ is analogous to the one presented in Section 6 for cmc surfaces in \mathbb{R}^3 . A sampling of curvature lines, a parameter q , and boundary angles, determine a hyperbolic orthogonal ring pattern and a spacelike two-sphere Koebe net. Our goal now is to reverse the construction of Theorem 10.4, and show how to recover a spacelike S_1 -cmc pair from its Gauss map.

The essential part of this construction is to determine the radii of vertex spheres and face circles for the surfaces in terms of data of the ring pattern, or the Koebe nets. We refer the reader to Figure 15 that illustrates the idea of the construction for the \mathbb{R}^3 case. Note that in our case horizontal edges always touch S_-^2 and vertical edges always touch S_+^2 , see Figure 23.

We consider a fundamental piece $[k_{v_s}, t_b^+, \tilde{k}_{v_c}, t_b^-]$ of the central extension k_{\boxplus} , defined in (34), of a spacelike two-sphere Koebe net. The piece consists of one vertex, one face center and two touching points, where the face center is determined by (35).

The edge lengths of the fundamental piece $[k_{v_s}, t_b^+, \tilde{k}_{v_c}, t_b^-]$ determine the radii of the vertex spheres and face circles, $d_{v_s}, d_{v_s}^*$ and $d_{v_c}, d_{v_c}^*$, cf. (36) - (38). The trigonometric

functions in (36) and (38) are replaced by the corresponding hyperbolic trigonometric functions.

For the radii of the resulting S_1 -cmc surface pair, expressed in terms of the γ -variables (66), we obtain

$$(68) \quad \begin{aligned} d_{v_s} &= \frac{1}{2} \frac{1}{\sqrt{q}} (\operatorname{dn} \gamma_{v_s} + q \operatorname{cn} \gamma_{v_s}), & d_{v_c} &= \frac{1}{2} \frac{1}{\sqrt{q}} \left(\frac{\operatorname{dn} \gamma_{v_c} + \operatorname{cn} \gamma_{v_c}}{\operatorname{sn} \gamma_{v_c}} \right), \\ d_{v_s}^* &= \frac{1}{2} \frac{1}{\sqrt{q}} (\operatorname{dn} \gamma_{v_s} - q \operatorname{cn} \gamma_{v_s}), & d_{v_c}^* &= \frac{1}{2} \frac{1}{\sqrt{q}} \left(\frac{\operatorname{dn} \gamma_{v_c} - \operatorname{cn} \gamma_{v_c}}{\operatorname{sn} \gamma_{v_c}} \right). \end{aligned}$$

We denote these radii by d_v and d_v^* , where the choice $v \in V_{\mathbb{S}}$ or $v \in V_{\mathbb{C}}$ determines whether we are considering vertex spheres or face circles.

The radii d_v and d_v^* determine the length of all edges of the (central extension of the) S_1 -cmc pair. The directions are determined by the edge parallelism to the two-sphere Koebe net. The following theorem ensures that the resulting spacelike surfaces with given edge lengths and directions exist. The proof is analogous to the proof of Theorem 6.1 for \mathbb{R}^3 .

Theorem 12.1. *Let $k_{\boxplus} : V(\mathcal{S}) \rightarrow \mathbb{R}^3$ be the central extension (34) of a spacelike two-sphere Koebe net. Then the $\mathbb{R}^{2,1}$ -valued discrete one-form ∂c_{\boxplus} defined by*

$$(69) \quad \partial_{(v,b)} c_{\boxplus} = d_v \frac{\partial_{(v,b)} k_{\boxplus}}{|\partial_{(v,b)} k_{\boxplus}|},$$

and the $\mathbb{R}^{2,1}$ -valued discrete one-form ∂c_{\boxplus}^* defined by

$$(70) \quad \partial_{(v,b)} c_{\boxplus}^* = \pm d_v^* \frac{\partial_{(v,b)} k_{\boxplus}}{|\partial_{(v,b)} k_{\boxplus}|},$$

with d_v and d_v^* given by (68), are exact. The signs (+) and (−) in (42) are chosen for horizontal and vertical edges, respectively. The integration of (69) and (70) defines the central extension of two surfaces c and c^* , which, when appropriately placed, form the center nets of a spacelike S_1 -cmc pair s, s^* with the Gauss map k_{\boxplus} . The vertex sphere radii and face circle radii of s and s^* are given by (68). The S_1 -cmc pair with the Gauss map k_{\boxplus} is unique up to translation.

Let us consider the case of a combinatorial rectangle. The Dirichlet and Neumann boundary data on V_B prescribe the metric or the cone angles on the boundary of the corresponding S_1 -cmc surface pair, respectively. Using Theorem 11.2 we can formulate the following general existence and uniqueness result.

Theorem 12.2. *For any Dirichlet or Neumann boundary data as in Theorem 11.2 there exists an unique spacelike S_1 -cmc pair s, s^* with these boundary metric or cone angles.*

13. MAXIMAL SURFACES IN THE LIMIT

Maximal surfaces in $\mathbb{R}^{2,1}$ are the natural analogues of minimal surfaces in \mathbb{R}^3 . Following the geometric characterization of S_1 -minimal surfaces as S_1 -isothermic surfaces that are Christoffel dual to Koebe nets [15], we will now introduce S_1 -maximal surfaces in $\mathbb{R}^{2,1}$, see also [4].

Definition 13.1. *An S_1 -maximal surface is an S_1 -isothermic surface whose Christoffel dual is a spacelike Koebe net.*

Analogous to the Euclidean case, we introduce a small parameter ϵ and consider an S_1 -cmc pair $\frac{1}{\epsilon}s, \frac{1}{\epsilon}s^*$ with $q = 1 - \epsilon$ and mean curvature $H = \epsilon$. Recall that the existence of s, s^* , as stated in the following Theorem, is a consequence of Theorem 12.2.

Theorem 13.2. *Consider a one parameter family of hyperbolic orthogonal ring patterns with $q = 1 - \epsilon$, fixed boundary conditions, and a limiting hyperbolic orthogonal circle pattern as $q \rightarrow 1$. Then there exists an ϵ -family of associated S_1 -cmc pairs, $\frac{1}{\epsilon}s$ and $\frac{1}{\epsilon}s^*$, with mean curvature $H = \epsilon$. In the limit $\epsilon \rightarrow 0$, s converges to a spacelike Koebe net with the edges touching the unit sphere, and $\frac{1}{\epsilon}s^*$ converges to its dual S_1 -maximal surface.*

Proof. To analyze the behavior of the surfaces, we examine how the vertex sphere radii (68) evolve in the limit $\epsilon \rightarrow 0$. The procedure is analogous to the one in the proof of Theorem 7.1. Due to

$$(71) \quad (\operatorname{dn} - q \operatorname{cn})(\operatorname{dn} + q \operatorname{cn}) = \epsilon(1 + q),$$

and the approximation (47), we find

$$(72) \quad a_{\operatorname{dn}} - a_{\operatorname{cn}} = \cosh(\gamma_v),$$

where $a_{\operatorname{cn}} := -\frac{\partial}{\partial q} \operatorname{cn}(\beta_v, 1)$ and $a_{\operatorname{dn}} := -\frac{\partial}{\partial q} \operatorname{dn}(\beta_v, 1)$. With this, we observe that the dual radii approach

$$\frac{1}{2} \cosh(\gamma_v),$$

while the primal radii go to infinity,

$$\frac{1}{\epsilon} \frac{1}{\cosh(\gamma_v)}.$$

The primal radii remain finite for the normalized surface $s = \epsilon \frac{1}{\epsilon}s$. Following the same reasoning as in Theorem 7.1, the two surfaces with vertex sphere radii $\cosh(\gamma_v)$ and $\frac{1}{\cosh(\gamma_v)}$ indeed form a spacelike Koebe net and an S_1 -maximal surface, respectively. \square

Remark. In the limit we obtain spacelike Koebe nets. Through a projective transformation, the spacelike unit sphere can be mapped to the unit sphere in \mathbb{R}^3 . Since Koebe nets are invariant under projective transformations, the image of a spacelike Koebe net under this projective transformation is a Koebe net whose edges are tangent to one half of the unit sphere in \mathbb{R}^3 . Conversely, by first applying a projective transformation that maps a Koebe net in \mathbb{R}^3 to tangent to half of the unit sphere in \mathbb{R}^3 , and then applying a transformation that maps the unit sphere of \mathbb{R}^3 to the unit sphere in $\mathbb{R}^{2,1}$, we obtain a spacelike Koebe net tangent to the upper half of the unit sphere in $\mathbb{R}^{2,1}$. Thus, the difference between the treatment of Euclidean minimal surfaces and Lorentz maximal surfaces lies only in the handling of boundary conditions.

14. EXAMPLES OF CMC SURFACES IN $\mathbb{R}^{2,1}$

By Theorem 12.2, we can construct S_1 -cmc surfaces in $\mathbb{R}^{2,1}$ from any given Neumann or Dirichlet boundary data.

In Figure 25 we present two examples: an S_1 -maximal surface with corresponding hyperbolic orthogonal circle pattern, and an S_1 -cmc surface with corresponding hyperbolic orthogonal ring pattern. Both surfaces are constructed using the same boundary data, specifically chosen so that the centers of the boundary circles or rings lie on a hyperbolic quadrilateral with ideal vertices.

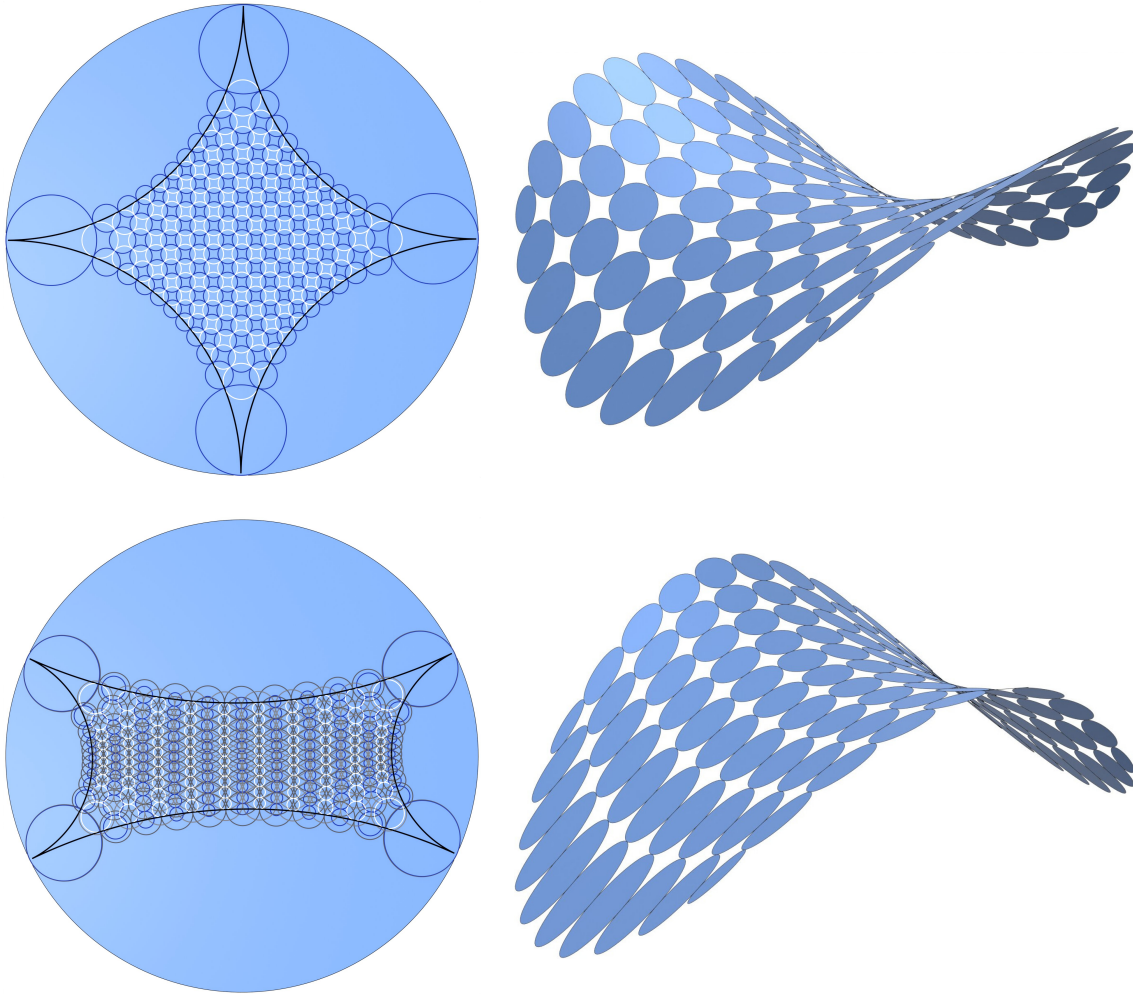


Figure 25. A hyperbolic orthogonal circle pattern ($q = .99999$) and the corresponding S_1 -minimal surface (top) and a hyperbolic orthogonal ring pattern ($q = 0.99$) with corresponding S_1 -cmc surface. The patterns are constructed using identical Neumann boundary data. The prescribed angles are approximately zero at the corners and π at the white boundary vertices which lead to hyperbolic quadrilaterals with ideal vertices.

REFERENCES

- [1] ADLER, V. E., BOBENKO, A. I., AND SURIS, Y. B. Classification of integrable equations on quad-graphs. The consistency approach. *Commun. Math. Phys.* 233, 3 (2003), 513–543.
- [2] ADLER, V. E., AND SURIS, Y. B. Q4: Integrable master equation related to an elliptic curve. *Int. Math. Res. Not.* 2004, 47 (2004), 2523–2553.
- [3] AFFOLTER, N. C., DELLINGER, F., MÜLLER, C., POLLY, D., AND SMEENK, N. Discrete Lorentz surfaces and s-embeddings I: isothermic surfaces, 2024. In preparation.
- [4] AFFOLTER, N. C., DELLINGER, F., MÜLLER, C., POLLY, D., AND SMEENK, N. Discrete Lorentz surfaces and s-embeddings II: maximal surfaces, 2024. In preparation.
- [5] AFFOLTER, N. C., AND TECHTER, J. Principal binets, 2024. arXiv:2409.11322.
- [6] BARBOT, T., CHARETTE, V., DRUMM, T., GOLDMAN, W. M., AND MELNICK, K. A primer on the (2+1) Einstein universe, 2007. arXiv:0706.3055.
- [7] BOBENKO, A., AND PINKALL, U. Discrete isothermic surfaces. *J. Reine Angew. Math.* 475 (1996), 187–208.
- [8] BOBENKO, A., AND SPRINGBORN, B. Variational principles for circle patterns and Koebe’s theorem. *Trans. Am. Math. Soc.* 356, 2 (2004), 659–689.
- [9] BOBENKO, A. I. Constant mean curvature surfaces and integrable equations. *Russ. Math. Surv.* 46, 4 (1991), 1–45.
- [10] BOBENKO, A. I., Ed. *Advances in discrete differential geometry*. Springer, [Berlin], 2016.
- [11] BOBENKO, A. I. Spherical and hyperbolic orthogonal ring patterns: integrability and variational principles, 2024. arXiv:2409.06573.
- [12] BOBENKO, A. I., BÜCKING, U., AND SECHELMANN, S. Discrete minimal surfaces of Koebe type. In *Modern approaches to discrete curvature*, vol. 2184 of *Lecture Notes in Math*. Springer, 2017, pp. 259–291.
- [13] BOBENKO, A. I., HELLER, S., AND SCHMITT, N. Constant mean curvature surfaces based on fundamental quadrilaterals. *J. Math. Phys. Anal. Geom.* 24 (2021), 1–46.
- [14] BOBENKO, A. I., AND HOFFMANN, T. S-conical CMC surfaces. Towards a unified theory of discrete surfaces with constant mean curvature. In *Advances in discrete differential geometry*. Springer, 2016, pp. 287–308.
- [15] BOBENKO, A. I., HOFFMANN, T., AND SPRINGBORN, B. A. Minimal surfaces from circle patterns: Geometry from combinatorics. *Ann. Math.* 164, 1 (2006), 231–264.
- [16] BOBENKO, A. I., NEWJOTO, J., AND TECHTER, J. Koebe polyhedra and minimal surfaces, 2019. Animation film, 7 min, www.discretization.de/movies.
- [17] BOBENKO, A. I., AND PINKALL, U. Discretization of surfaces and integrable systems. In *Discrete integrable geometry and physics*, A. Bobenko and R. Seiler, Eds., vol. 16 of *Oxford Lecture Ser. Math. Appl.* Oxford Univ. Press, New York, 1999, pp. 3–58.
- [18] BOBENKO, A. I., POTTMANN, H., AND WALLNER, J. A curvature theory for discrete surfaces based on mesh parallelity. *Math. Ann.* 348 (2010), 1–24.
- [19] BOBENKO, A. I., SCHRÖDER, P., SULLIVAN, J. M., AND ZIEGLER, G. M., Eds. *Discrete differential geometry*, vol. 38 of *Oberwolfach Seminars*. Birkhäuser Verlag, Basel, 2008.
- [20] BOBENKO, A. I., AND SURIS, Y. B. *Discrete differential geometry. Integrable structure*, vol. 98 of *Graduate Studies in Mathematics*. AMS, Providence, RI, 2008.
- [21] BRIGHTWELL, G. R., AND SCHEINERMAN, E. R. Representations of planar graphs. *SIAM J. Discrete Math.* 6, 2 (1993), 214–229.
- [22] CIEŚLIŃSKI, J., GOLDSTEIN, P., AND SYM, A. Isothermic surfaces in \mathbf{E}^3 as soliton surfaces. *Phys. Lett. A* 205, 1 (1995), 37–43.
- [23] CRANE, K., Ed. *An excursion through discrete differential geometry*, vol. 76 of *Proceedings of Symposia in Applied Mathematics*. AMS, Providence, RI, 2020.
- [24] DORFMEISTER, J., PEDIT, F., AND WU, H. Weierstrass type representation of harmonic maps into symmetric spaces. *Comm. Anal. Geom.* 6, 4 (1998), 633–668.

- [25] GROSSE-BRAUCKMANN, K., KUSNER, R. B., AND SULLIVAN, J. M. Triunduloids: embedded constant mean curvature surfaces with three ends and genus zero. *J. Reine Angew. Math.* 564 (2003), 35–61.
- [26] GROSSE-BRAUCKMANN, K., AND POLTHIER, K. Compact constant mean curvature surfaces with low genus. *Exp. Math.* 6, 2 (1997), 13–32.
- [27] GU, D., AND SAUCAN, E. *Classical and Discrete Differential Geometry: Theory, Applications and Algorithms*. CRC Press, 2023.
- [28] HELLER, L., HELLER, S., AND SCHMITT, N. Navigating the space of symmetric cmc surfaces. *J. Differ. Geom.* 110, 3 (2018), 413–455.
- [29] HELLER, L., HELLER, S., AND TRAIZET, M. Area estimates for high genus Lawson surfaces via DPW. *J. Differ. Geom.* 124, 1 (2023), 1–35.
- [30] HERTRICH-JEROMIN, U. *Introduction to Möbius differential geometry*, vol. 300 of *London Math. Soc. Lecture Note Ser.* Cambridge Univ. Press, 2003.
- [31] HERTRICH-JEROMIN, U., HOFFMANN, T., AND PINKALL, U. A discrete version of the Darboux transform for isothermic surfaces. In *Discrete integrable geometry and physics*, vol. 16 of *Oxford Lecture Ser. Math. Appl.* Oxford Univ. Press, New York, 1999, pp. 59–81.
- [32] HERTRICH-JEROMIN, U., AND PEDIT, F. Remarks on the Darboux transform of isothermic surfaces. *Documenta Math.* 2 (1997), 313–333.
- [33] HITCHIN, N. J. Harmonic maps from a 2-torus to the 3-sphere. *J. Differ. Geom.* 31, 3 (1990), 627–710.
- [34] HOFFMAN, D., AND KARCHER, H. Complete embedded minimal surfaces of finite total curvature. In *Geometry V: Minimal surfaces, Encyclopedia of Mathematical Sciences*, R. Osserman, Ed., vol. 90. Springer, 1997, pp. 5–93.
- [35] HOFFMANN, T. A Darboux transformation for discrete s-isothermic surfaces. *J. Math-for-Ind.* 2 (2010), 157–169.
- [36] INOBUCHI, J.-I. Surfaces in Minkowski 3-space and harmonic maps. In *Harmonic morphisms, harmonic maps, and related topics*, vol. 413 of *Chapman & Hall/CRC Res. Notes Math.* Boca Raton, FL, 2000, pp. 249–270.
- [37] KARCHER, H. The triply periodic minimal surfaces of Alan Schoen and their constant mean curvature companions. *Manuscripta mathematica* 64, 3 (1989), 291–357.
- [38] KOEBE, P. Kontaktprobleme der konformen Abbildung. *Abh. Sächs. Akad. Wiss. Leipzig* 88 (1936), 141–164.
- [39] KÖNIG, B. A geometric construction for the associated family of S-isothermic cmc surfaces, 2018. PhD thesis, TU München.
- [40] LAN, S.-Y., AND DAI, D.-Q. C^∞ -convergence of circle patterns to minimal surfaces. *Nagoya Math. J.* 194 (2009), 149–167.
- [41] LAWSON JR, H. B. Complete minimal surfaces in S^3 . *Ann. Math.* (1970), 335–374.
- [42] LIU, Y., POTTMANN, H., WALLNER, J., YANG, Y.-L., AND WANG, W. Geometric modeling with conical meshes and developable surfaces. In *ACM SIGGRAPH 2006 Papers* (2006), pp. 681–689.
- [43] MILNOR, T. K. Harmonic maps and classical surface theory in Minkowski 3-space. *Trans. Am. Math. Soc.* 280, 1 (1983), 161–185.
- [44] NIST digital library of mathematical functions: Chapter 22 Jacobian elliptic functions. <https://dlmf.nist.gov/22> [Accessed: (11.10.2024)].
- [45] POTTMANN, H., AND WALLNER, J. The focal geometry of circular and conical meshes. *Adv. Comp. Math.* 29 (2008), 249–268.
- [46] RIVIN, I. A characterization of ideal polyhedra in hyperbolic 3-space. *Ann. of Math.* 143, 1 (1996), 51–70.
- [47] SCHOEN, A. H. *Infinite periodic minimal surfaces without self-intersections*, vol. 5541. National Aeronautics and Space Administration, 1970.
- [48] SCHRAMM, O. How to cage an egg. *Inventiones mathematicae* 107, 1 (1992), 543–560.
- [49] SCHRAMM, O. Circle patterns with the combinatorics of the square grid. *Duke Math. J.* 86, 2 (1997), 347–389.
- [50] SCHWARZ, H. A. *Gesammelte mathematische Abhandlungen*, vol. 260. AMS, 1972.

- [51] SPRINGBORN, B. A. Variational principles for circle patterns, 2003. arXiv:math/0312363.
- [52] TELLIER, X., HAUSWIRTH, L., DOUTHE, C., AND BAVEREL, O. Discrete cmc surfaces for doubly-curved building envelopes. In *Advances in Architectural Geometry* (2018).
- [53] TRAZET, M. Construction of constant mean curvature n-noids using the DPW method. *J. Reine Angew. Math.* 2020, 763 (2020), 223–249.

ALEXANDER I. BOBENKO, NINA SMEENK
INSTITUTE OF MATHEMATICS, SECR. MA 8-3, TU BERLIN, 10623 BERLIN, GERMANY
EMAIL: {bobenko,smeenk}@math.tu-berlin.de

TIM HOFFMANN
DEPT. OF MATHEMATICS, TU MUNICH, 85748 GARCHING, GERMANY
EMAIL: hoffmant@ma.tum.de